MOLECULAR BEAM EPITAXIAL GROWTH OF ZnSe ON (211)B GaAs

A Thesis Submitted to
Graduate School of Engineering and Sciences of
İzmir Institute of Technology
in Partial Fulfillment of the Requirements for the Degree of

MASTER OF SCIENCE

in Material Science and Engineering

by
Begüm YAVAŞ

June 2017
İZMİR

We approve the thesis of **Begüm YAVAŞ**

Examining Committee Members:

Assoc. Prof. Dr. Serkan ATEŞ
Department of Physics, İzmir Institute of Technology

Assoc. Prof. Dr. Uğur SERİNCAN
Department of Physics, Anadolu University

Assoc. Prof. Dr. Özgür ÇAKIR
Department of Physics, İzmir Institute of Technology

09 June 2017

Assoc. Prof. Dr. Serkan ATEŞ
Supervisor, Department of Physics,
İzmir Institute of Technology

Prof. Dr. Serdar ÖZÇELİK
Co-Supervisor, Department of Chemistry,
İzmir Institute of Technology

Prof. Dr. Mustafa M. DEMİR
Head of the Department of Material Science and Engineering

Prof. Dr. Aysun SOFUOĞLU
Dean of Graduate School of Engineering and Science

ACKNOWLEDGEMENTS

I would like to first thank my parents for their endless support and patient during the all of my study.

I would like to thank the late my advisor Assoc. Prof. Dr. Yusuf Selamet for all his support and patience. Thanks to him, I have chance to study in this interesting study area and learn many new detailed of my study. I always remember him with his nice help and cheerful.

I would like to thank my advisor Assoc. Prof. Dr. Serkan Ateş for all his help and patience. I have been able to complete this study with his support and guidance.

I would like to thank other committee members of my thesis committee Assoc. Prof. Dr. Uğur Serincan and Assoc. Prof. Dr. Özgür Çakır for their participation and comments. And also I would like to thank my co-advisor Prof. Dr. Serdar Özçelik.

I also would like to thank my colleagues and friends helped me to complete during all process of my study. Especially, I am very thankful Elif Bilgilisoy for her great friendship, support and patience. She always helped me and motivated me whole process of my study. I am also very thankful Hasan Aydın for his great friendship and for AFM measurement. I would like to thank Ozan Arı for MBE growth and XRD measurements. I would like to thank for her great friendship and ex-situ SE measurements. I would like to thank Elif Özçeri for Raman measurements and Emine Bakali for SEM measurements. In addition, I would like to thank Hazan Özkan, Barış Akbalı and Alper Yanılmaz for friendship and support.

I also very thankful to Serkan Aydın who always supported me and encouraged me through whole my study.

Lastly, I wish to acknowledge ASELSAN and SSM for financial and technical facilities in our laboratory.

ABSTRACT

MOLECULAR BEAM EPITAXIAL GROWTH OF ZnSe ON (211)B GaAs

The Mercury Cadmium Telluride ($Hg_{1-x}Cd_xTe$) play important role for infrared (IR) focal plane array application. It is grown on variety alternative substrates which are Si, Ge, GaAs or GaSb. When GaAs is compared with the others alternative substrate, it is more preferable due to having good surface polarity and also easily commercially available of high quality. When HgCdTe epilayer is grown directly on the GaAs substrate, there exist some dislocations in the epilayer due to large lattice mismatch between HgCdTe and GaAs substrate.The CdTe semiconductor is grown like a buffer layer to reduce dislocation in the HgCdTe epilayer grown on GaAs or other alternative substrate [1].The crystal quality of CdTe buffer layer directly affected HgCdTe epilayer. Therefore, CdTe needed to be low defect density.Because of %14.6 lattice mismatch between CdTe and GaAs [2], some defects are observed in CdTe buffer layer. ZnSe epilayer can be used to decrease lattice mismatch between CdTe and alternative substrate. When ZnSe interlayers are grown with high quality, CdTe affects positively.

The aim of this theses is the growth of ZnSe epilayer films on (211) GaAs substrates by molecular beam epitaxy (MBE). The effect of growth temperature, VI/II flux ratio and deoxidation process with In and As were studied in this study. Crystal qualities of films were investigated by using X-ray diffraction. The surface morphology of ZnSe films were analyzed by atomic force microscopy and Nomarski microscopy. Vibrational phonon modes, thermal and elastic strains of ZnSe epilayer were observed by using Raman spectroscopy [3].

ÖZET

ZnSe'ın (211)B GaAs ÜZERİNE MOLEKÜLER DEMET EPİTAKSİYEL BÜYÜTÜLMESİ

Cıva Kadmiyum Tellür (HgCdTe), kızılötesi fokal düzlem dizini uygulamaları için önemli bir rol oynar. Si, Ge, GaAs ya da GaSb gibi çeşitli alt-tabanlar üzerine büyütülebilir. GaAs iyi bir yüzey polaritesine ve bunun yanında yüksek kalitede ticari olarak bulunduğu için, diğer alt-tabanlar ile kıyaslandığı zaman daha çok tercih edilir. HgCdTe filmi direk olarak GaAs yüzeyine büyütüldüğün de, HgCdTe ile GaAs arasında büyük örgü uyumsuzluğu olduğu için HgCdTe bazı dislokasyonlar oluşur. GaAs yüzeyine ya da diğer alt-tabanlar üzerine büyütülen HgCdTe de oluşan dislokasyonları düşürmek için, CdTe yarıiletkeni HgCdTe ve GaAs arasına tampon katman olarak büyütülür. CdTe tampon katmanın kristal kalitesi HgCdTe'ı doğrudan etkiler. Bu yüzden CdTe düşük kusur yoğunluğuna sahip olmalıdır. GaAs ve CdTe örgü uyumsuzluğu %14.6 olduğu için, CdTe tampon katmanında bazı kusurlar gözlemlenir. ZnSe ara katmanı CdTe ve alt-tabanlar arasındaki örgü uyumsuzluğunu düşürmek için kullanılabilir. ZnSe ara katmanı yüksek kalitede büyütüldüğü zaman, CdTe filmi pozitif olarak etkilenir.

Bu tezin amacı ZnSe ara katmanının GaAs(211)B yüzeyine Moleküler Demet Epitaksiyel (MBE) ile büyütülmesidir. Bu çalışmada, büyütme sıcaklığı, VI/II akı oranı, In ve As ile yapılan deoksidasyon adımları çalışılmıştır. Filmlerin kristal kalitesi X-ışın kırınımı (XRD) ile tahmin edilmiştir. Yüzey morfolojisi atomik kuvvet mikroskobu ve Nomarski mikroskobu ile analiz edilmiştir. ZnSe ara katmanının titreşimli fonon modları, termal ve elastik gerilimleri Raman spektroskobisi kullanılarak gözlemlenmiştir.

TABLE OF CONTENTS

LIST OF FIGURES

Figure **Page**

LIST OF TABLES

Table **Page**

LIST OF ABBREVIATIONS

AFM	Atomic Force Microscopy
BCC	Body Centered Cubic
CdTe	Cadmium Telluride
ZnSe	Zinc Selenide
CdZnTe	Cadmium Zinc Telluride
EPD	Etch Pit Density
FCC	Face Centered Cubic
FTIR	Fourier Transformation Infrared
FWHM	Full Width at Half Maximum
GaAs	Gallium Arsenide
IR	Infrared
LWIR	Long Wavelength Infrared
MBE	Molecular Beam Epitaxy
HgCdTe	Mercury Cadmium Telluride
MWIR	Mid Wavelength Infrared
ROIC	Read Out Integrated Circuit
SE	Spectroscopic Ellipsometry
SEM	Scanning Electron Microscopy
SC	Simple Cubic
SWIR	Small Wavelength Infrared
VC	Very Cheap
C	Cheap

CHAPTER 1

INTRODUCTION

The ternary alloy Mercury Cadmium Telluride ($Hg_{1-x}Cd_xTe$) is important material for infrared (IR) imaging. The short wavelength IR (SWIR=1–3 μm), mid-wavelength IR (MWIR= 3–5 μm), long wavelength IR (LWIR = 8- 14 μm) and very long wavelength IR (VLWIR= 14–30 μm) are produced with changing Cd composition which happens in HgCdTe [4].

HgCdTe was firstly grown on bulk $Cd_{1-x}Zn_xTe$ in mid-1980s, these material was preferred a substrate due to low lattice mismatch and very low thermal expansion coefficient with HgCdTe. Although these looks like advantage, CdZnTe have some disadvantages which are high cost, lack of uniformity on large area, very brittle material and large thermal mismatch with Si readout integrated circuit (ROIC) [5]. So, new alternative substrates need to grow high quality HgCdTe materials. Besides CdZnTe, Si, GaAs and Ge are used like alternative substrates in recent years [6-9]. They are low cost material and available large area when compared to CdZnTe. However, there are large lattice mismatch between HgCdTe and these alternative substrates. So CdTe buffer layer is grown to reduce lattice mismatch between alternative substrate and HgCdTe. The buffer surface defects affect performance of detector and focal plane array HgCdTe grown on them [10]. Therefore the crystal quality of CdTe buffer layer is important to obtain suitable HgCdTe infrared devices.

According to some studies, interlayers like ZnSe, CdSe and ZnTe [11] were grown to reduce lattice mismatch between CdTe buffer layer and alternative substrate. Thanks to this method, structural quality of CdTe buffer layer can be improved and strain of samples can be reduced. Hence, HgCdTe is affected positively.

In this study, GaAs (211)B was used like alternative substrate. ZnSe was grown as interlayer, due to it has lower lattice mismatch with GaAs (211)B when compared to ZnTe. Firstly ZnSe interlayer was grown on GaAs (211)B substrate by using molecular Beam Epitaxy (MBE). After that, *in-situ* spectroscopic ellipsometer was used to obtain film thickness and X-ray Diffraction (XRD), Atomic force microscopy (AFM), Nomarski and Raman were used to characterize the film quality.

- In Chapter 2, gives information about ZnSe properties. Besides this, alternative substrate for epitaxial growth of ZnSe will be given.
- In Chapter 3, introduce epitaxial growth techniques which are molecular beam epitaxy (MBE), Metalorganic Vapour Phase Epitaxy (MOVPE), Atomic Layer Epitaxy (ALE) and Pulse Laser Deposition (PLD).
- In Chapter 4, experimental techniques and procedures which are MBE system, X-ray Diffraction (XRD), Spectroscopic Ellipsometry (SE), Atomic Force Microscopy (AFM), Nomarski and Raman Spectroscopy are explained in detail.
- In Chapter 5, experimental results and discussion of epitaxial grown ZnSe nucleation layer are given. Firstly, informations about growth parameters are given. Then crystal quality is obtained by using XRD. Film thickness of ZnSe is measured with Spectroscopic Ellipsometry. AFM, Nomarski and Raman Spectroscopy are used to characterize ZnSe nucleation layer.
- In Chapter 6, summary of results, conclusion and future work are given.

CHAPTER 2

ZINC SELENIDE PROPERTIES

2.1. Crystal Structure

2.1.1. Crystal Lattice

The properties of solids depend on crystal structure of material. The arrangement of atoms, ions or molecules play important role to find properties of materials. An identical crystal is formed by small identical group of repetition atoms. This group is called basis. The basis is setted a mathematical point which is called lattice. ZnSe epilayers have zinc-blende crystal structure. Except for zinc-blende structure, simple cubic (SC), body-centered cubic (BCC) and face-centered cubic (FCC) structures will be discussed.

2.1.1.1. Simple Cubic Lattice

In simple cubic, single type of atoms are arranged (0,0,0) and distance between atoms are equal (Figure 1). The distances between each of them are defined lattice parameter and also dimension of smallest structure is referred with lattice parameter in the crystal lattice. The small structure is called unit cell. Combination of unit cell generates crystal structure. The example of SC is only Polonium (Po) crystal [12].

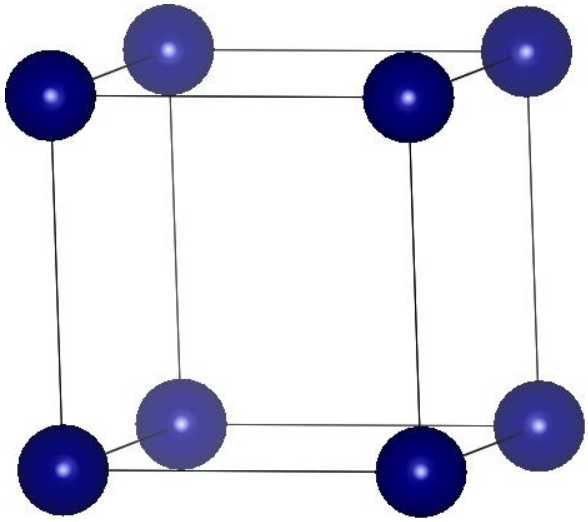

Figure 1. Simple cubic lattice structure [13]

Each of atoms lay different crystal axis so they are specified by coordinates of points like lattice constant a_1, a_2, a_3. However orientation of crystal plane is analysed different argument. The intersects are found on the lattice axis with lattice constant as h a_1, k a_2, l a_3 (h, k and l are intersect points). 1/h,1/k and 1/l are known reciprocal values of intersect point. The miller indices have different meaning. These are [hkl] refer direction of lattice vector, (h,k,l) refers lattice plane. Negative Miller indices values are shown as ā or –a.

2.1.1.2. Body Centered Cubic Lattice

Atoms are located eight corners and a single atom at the cube of center in BCC lattice structure Figure 2. It contains two atoms in unit cell. The coordination of atoms are (0, 0, 0) and (1/2, 1/2, 1/2). The most common example of BCC is Iron (Fe) crystal [14].

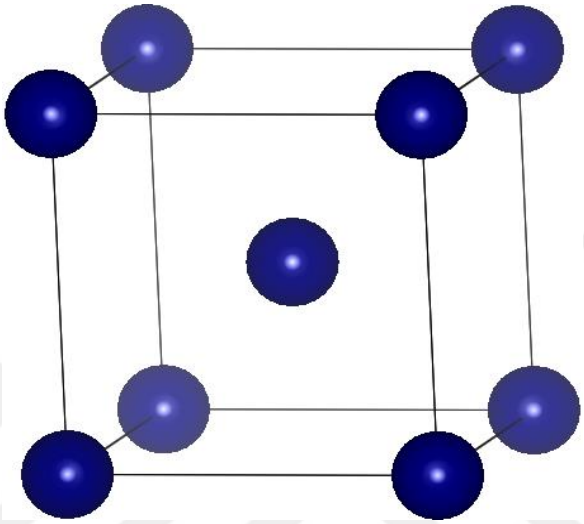

Figure 2. Body Centered Lattice Structure [13]

2.1.1.3. Face Centered Cubic Lattice

Atoms are located each of the corners and each centers of the all cubic Figure 3. BCC contains four atoms in unit cell. The coordination of atoms are (0, 0, 0), (0, 1/2, 1/2), (1/2, 0, 1/2) and (1/2, 1/2, 0). The most common example of FCC is NaCl [15].

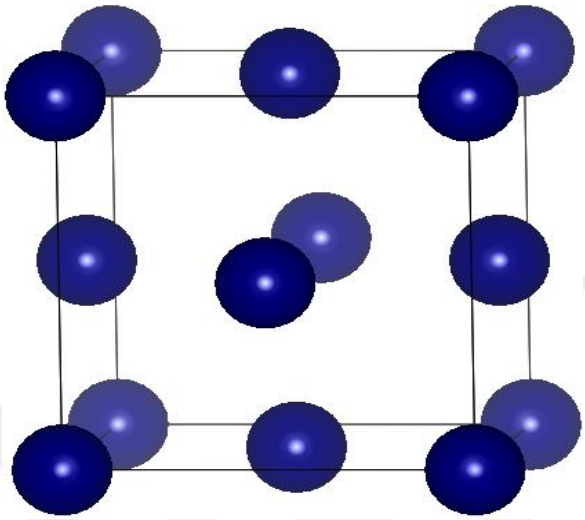

Figure 3.Face Centered Lattice Structure [13]

2.1.1.4. Zinc-Blende Lattice

In diamond, each carbon atom is bonded to another carbon atom. However in the Zinc-Blende structure, each atom bonded different species of atom. Like Diamond, zinc-blende lattice consist of two FCC lattice where one lattice is offset ¼ of unit cell. ZnSe has zinc-blende lattice structure. The coordinates of Se atoms are (0, 0, 0), (0, 1/2, 1/2), (1/2, 0, 1/2) and (1/2, 1/2, 0) and Zn atoms are (1/4, 1/4, 1/4), (1/4, 3/4, 3/4), (3/4, 1/4, 3/4) and (3/4, 3/4, 1/4). The combination of these two FCC lattice creates ZnSe lattice structure Figure 4.

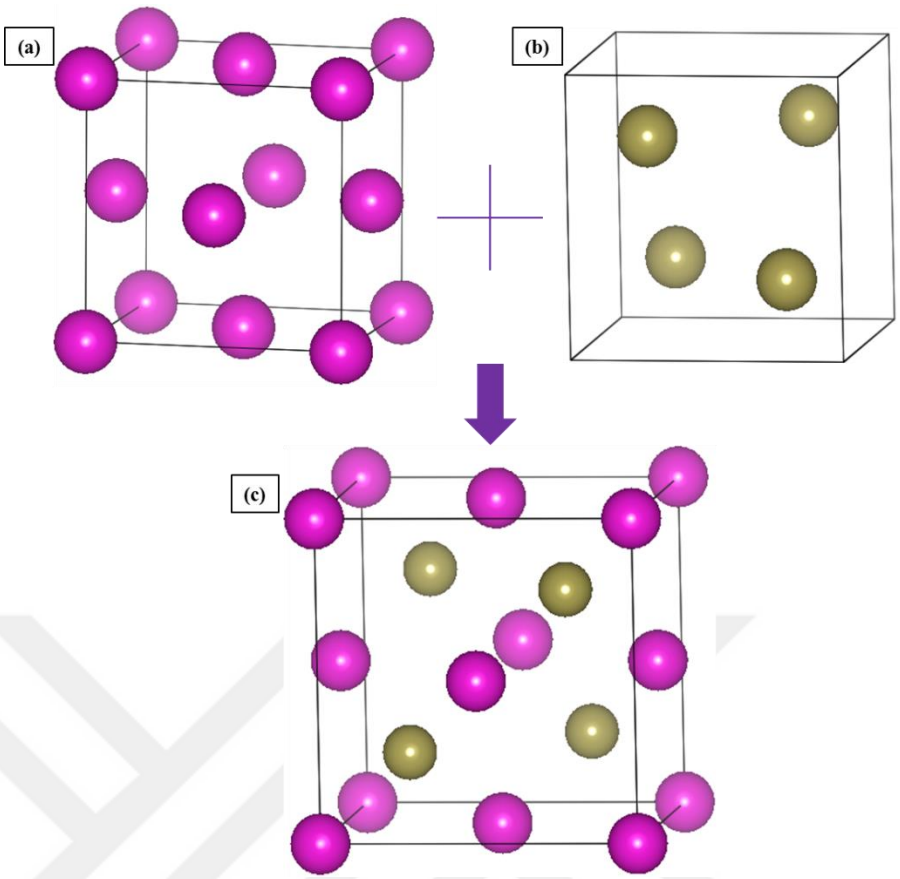

Figure 4. The combination of zinc-blende lattice structure of ZnSe with FCC (a) Se atoms and (b) Zn atoms [13]

2.2. Material Properties of Zinc Selenide

ZnSe has zinc-blende lattice structure with zinc and selenium atoms which are located on distinct face-centered cubic lattice. Because of the large differences electronegativity between Zn and Se atoms, Zn-Se bond has more ionic character than covalent. Bonding of Zn and Se atoms is calculated and %63 ionic component are found [16].The polar nature of ZnSe is that electron are localized Se anion. According to band structure, large electron and hole effective masses is resulted by tighter binding. ZnSe has direct band gap and is 2.67 eV at room temperature. Table 1 and Table 2 give some information about electrical and optical properties of ZnSe and some selected mechanical properties of ZnSe, respectively.

Table 1. Some electrical and optical properties of ZnSe [17-22]

Property	**Symbol**	**Value**	**Units**
Energy Gap (R.T)	E_g	2.8	eV
Electron effective mass	m_h	0.17	m_o
Hole effective mass	m_e	0.6	m_o
Electron Mobility (R.T)	μ_e	600	$cm^2/V.cm$
Hole Mobility (R.T)	μ_{hh}	~30	$cm^2/V.cm$
LO Phonon Frequency	w_{LO}	3.19	meV
Dielectric Constant	$\varepsilon_r(0)$	9.1	$\varepsilon_r(\varepsilon_o)$

Table 2. Some mechanical properties of ZnSe [22]

Property	**Symbol**	**Value**	**Units**
Lattice Constant	a_o	5.66	A^o
Expansion Coefficient	α	7.00	$10^{-6}/^oC$
Melting Point	M_p	1520	^oC
Thermal Conductivity	K	0.19	W/cm.K
Elastic Constants	C_{11} C_{12}	8.59 5.06	10^{10} dyne/cm^2 10^{10} dyne/cm^2

2.3. Alternative Substrate for Epitaxial Growth of Zinc Selenide

The lattice and thermal expansion coefficient matched between ZnSe epilayer and alternative substrate are crucial areas [23, 24]. Homoepitaxial growth is suitable to satisfy the matching of lattice constant and thermal expansion coefficient. However, a large and good-quality ZnSe single-crystal substrate has not been available[25].ZnSe epilayer have been grown heteroepitaxially on substrates materials such as GaAs [26, 27], Si [28, 29] and Ge [30].

Table 3. Si, Ge and GaAs substrate properties for ZnSe epilayer *[27, 31, 32]*

	Si	Ge	GaAs
Melting Temp. (^{o}C)	1412	937	1237
Thermal Conductivity (mW/(cmK)	1235	580	500
Vickers Hardness(kg mm^{-2}) 300K	1150-1330	780	360
Crystal Structure	Diamond	Diamond	ZB
Lattice Constant (Å)	5.43	5.66	5.65
Lattice Mismatch with ZnSe (%)	4.3	0.19	0.27
Etch Pit Density (cm^{-2})	10-100	5x10^{3}	10^{3}
The limit value of Rocking Curve Width (arcsec)	7	10	14
Thermal Expansion Coefficient (10^{-6} K^{-1})	2.6	5.9	6.7
Thermal Expansion Mismatch (%)	92.3	-55.9	-11.9
Max. Available Size	15” Ø	6” Ø	6” Ø
Cost	VC	C	C

Table 3 shows the comparison between alternative substrates and ZnSe which is lattice constant 5.67 A^o and thermal expansion coefficient 7×10^{-6} C^{-1} .Si substrates are low-cost, large area and have better thermal and mechanical properties than GaAs substrates. However, the large lattice mismatch (4.3 %) between ZnSe and Si and also chemical reaction at the interface make the growth of ZnSe on Si difficult [28, 33, 34]. When the ZnSe are grown on Si, $SiSe_x$ interlayer happen between these two materials [34].

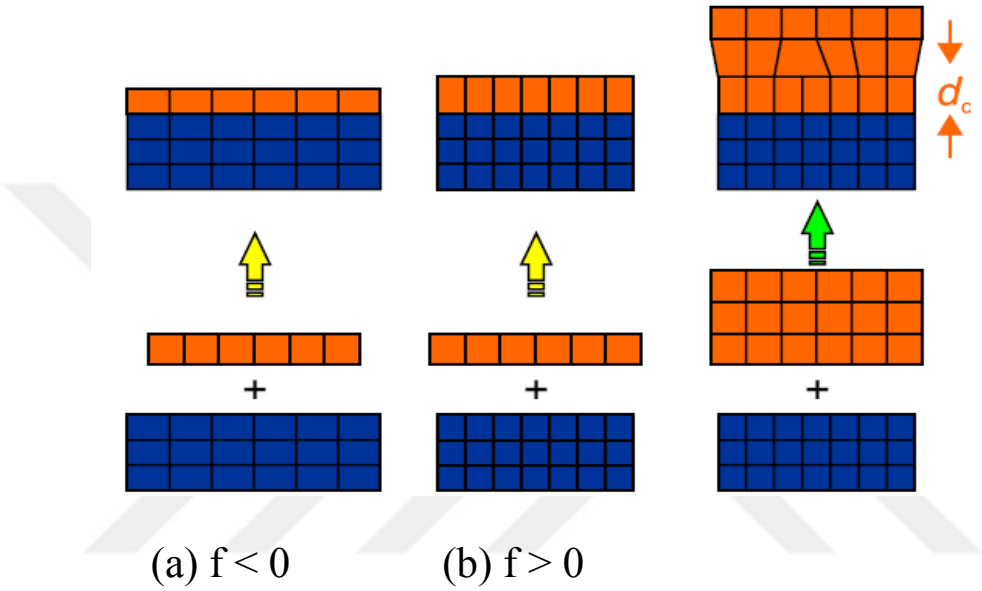

Figure 5. Heteroepitaxial thin film growth can result in strain as a result of the lattice mismatch f. (a) lattice-matched, (b) compressive and tensile strain, (c) relaxed thin film growth for a thickness > dc. [35]

The heteroepitaxial growth needs growth of thin film on suitable substrate. There can be difference between film and substrate in terms of lattice constant. Because of this reason, growing film has some deformation which will affect its optical properties. The lattice mismatch defines as;

$$f = \frac{2(a_f - a_s)}{(a_f - a_s)} \sim \frac{a_f - a_s}{a_s} \qquad (2.1)$$

Where a_f and a_s represent lattice constant of film and substrate, respectively. In Figure 5, when f is smaller than zero, tensile strain of film happen in the plane direction. However when f is bigger than zero, compressive strain happen out-of-plane direction. If film thickness exceeds critical thickness of film (d_c), the film will be relaxed.

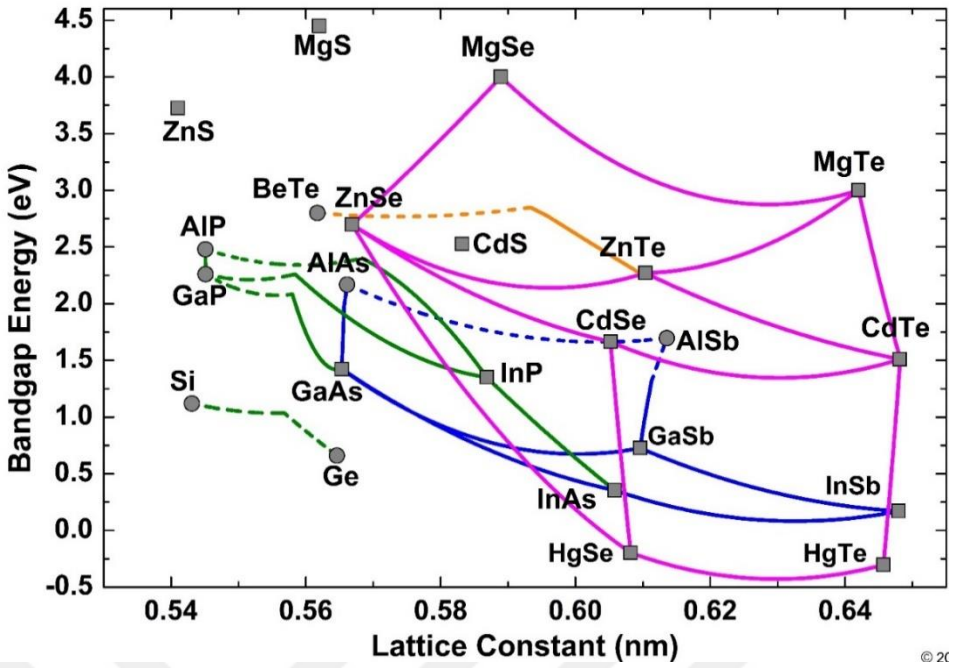

Figure 6. Energy gap versus lattice parameter for several semiconductor materials [36].

In Figure 6, the lattice parameters of semiconducting materials and alternative substrates are given. As seen from the graph, Ge has small lattice mismatch to ZnSe. It can be suitable substrate for growing ZnSe/Ge heteroepitaxial [37]. However, the major difficulties are encountered while growing ZnSe on Ge. These are antiphase disorder and interface excess charges [38-40]. ZnSe is polar and Ge is nonpolar. Because of this reason, antiphase disorder are seen at the interface [30].

Even if substrate is lattice-matched with growth film, substrate and film will have most probably different thermal expansion coefficient α(T). Due to change of temperature, strain will produce in the film. We can divide two cases of lattice + thermal strain. The first case is that $d < h_c$ where d is the final thickness of film and h_c is critical thickness of film. Strain of film can be given as a function of temperature:

$$\varepsilon_{//}(T) = \frac{a_s(T) - a_0(T)}{a_0(T)} \tag{2.2}$$

Where a_0 and a_s are lattice constants of film and substrate, respectively.

In the second case, if film thickness bigger than critical thickness, it grows as relax at growth temperature.

$$\varepsilon_{//}(T_g) = \frac{a_{//}(T_g) - a_0(T_g)}{a_0(T_g)} \cong 0 \quad (2.3)$$

Now we can write lattice constant of freestanding film with expansion coefficient $\alpha_F(T)$.

$$a_0(T) = a_0(T_g)[1 + \int_{T_g}^{T} \alpha_F(T)dT \quad (2.4)$$

And when film adhered on the substrate, lattice constant of film can be written,

$$a_{//}(T) = a_0(T_g)[1 + \int_{T_g}^{T} \alpha_S(T)dT \quad (2.5)$$

Where T is temperature and T_g is growth temperature.

In this equation, $\alpha_s(T)$ is used because thick substrate more dominant than thin film. So we can write thermal strain,

$$\varepsilon_{//}(T) = \frac{\int_{T_g}^{T}[\alpha_s(T) - \alpha_F(T)]dT}{1 + \int_{T_g}^{T} \alpha_F(T)dT} \quad (2.6)$$

When thermal expansion of film is bigger than substrate ($\alpha_F > \alpha_S$), there are two possibilities ZnSe grown on GaAs. First one is, if $T < T_g$ after $\varepsilon_{//}$ is bigger than zero and tensile biaxial stress happen. Second is, if $T > T_g$ then $\varepsilon_{//}$ is smaller than zero and biaxial compression happen. We conclude that this result is independent lattice mismatch.

GaAs has also small lattice mismatch to ZnSe (0.27 %). It has been a good substrate of choice to grow ZnSe epitaxial layer [38]. When GaAs substrate is compared to Ge substrate, ZnSe grown on GaAs has higher quality despite the larger lattice mismatch [25, 41]. Existence of antiphase domains and misorientation in the grown ZnSe epilayer on Ge affect crystal quality negatively [25]. For all above mentioned reasons, GaAs is the ideal substrate for growing ZnSe epilayer.

The polarity of GaAs substrate is defined as As-terminated (Ga) and B-terminated (As) substrate. As rich surface (B) can be preferred for growth of II-VI buffer layer without any nucleation process which is necessary for Si and Ge [42, 43]. According to research, (211)B growth is preferred due to suppressing twin formation,

minimizing macroscopic defects and having high sticking coefficient. (211) orientation consists of (100) steps and (111) terraces. This step surface allows sticking of atoms which have low sticking coefficient.

2.4. Zinc Selenide Application

II-VI compound semiconductors have been interested with much attention since ZnSe-based blue-green laser diodes were first displayed. Zinc selenide is II - VI semiconducting material with a direct and wide band gap of 2.7 eV at room temperature.[44]For this reasons ZnSe is thought that is to fabricate efficient emitters such as light emitting diodes and laser diodes in the blue region of the visible spectrum [23, 45].

Since the first expression of ZnSe-based blue-green laser diodes was displayed in 1991,significant intention have been made to improve their performance in order to obtain long lasting devices at room temperature. ZnSe/GaAs heterostructure promise wide application in optoelectronic and microelectronic devices[23, 46].Such as the high quality ZnSe single crystals ,as a substrate for homoepitaxial growth, is very important for the development of II-VI blue light-emitting diodes(LEDs) or blue laser diodes (LDs) [47].

ZnSe is also used as a window layer for the fabrication of thin film solar cells. It is mainly used as a protective and antireflection coating for infrared-operating electrochromic thermal-control surfaces because its large band gap permits a large number of photons to reach the absorber layer [48]. The synthesis of binary metal chalcogenides of group II - VI semiconductors in a nano crystalline form has been a rapidly growing area of research due to their important non-linear optical properties, photoluminescent and electroluminescent properties, crystalline size effect or quantum size effect, and other important physical and chemical properties [2].

The other II-VI compound ZnTe has also many promising applications in optoelectronic devices in the blue-green spectral region [49]. ZnTe are grown directly on GaAs[50, 51].However, while these processing happen, some problems exhibit due to cross doping effects from interdiffusion in the interfacial region [52-54] or due to strain effects from lattice mismatch between II-VI epilayers and the III-V substrates [55]. Consequently, ZnTe/GaAs heterostructures have difficulties for obtaining high

quality ZnTe due lattice mismatch (7.6 % 300K) and thermal expansion coefficient difference (44.8 % 300K). ZnSe buffer layer have been grown to reduce strain effects on GaAs before ZnTe growth. By using these growth method, ZnTe epitaxial films which are grown on GaAs with ZnSe buffer layer give promise for potential application in optoelectronic devices operating [49].

The substrate choice is very important for good quality MBE growth of CdTe and HgCdTe. Because, the crystal quality of this films play important role for performance of MCT_based infrared (IR) detectors and focal – plane arrays (FPAS). Crystal quality of CdTe is primary factor for growth HgCdTe. Therefore, CdTe buffer layer must have low defect density. One reason of defects are lattice mismatch. ZnSe interlayer can be used to decrease lattice mismatch between CdTe and alternative substrate. When ZnSe interlayer is grown with high quality, CdTe affects positively.

2.5. Literature Review

ZnSe was grown on different GaAs substrates which were (100), (110), (111), (001) [27, 56, 57]. Growth temperature, flux ratio (VI/II) and critical thickness are important to have good surface morphology and crystal quality of ZnSe.

The effect of GaAs surface stoichiometry was examined on crystal and surface quality of ZnSe layer. Y. Qiu and his group were prepared two types surface [56]. These were Se-rich surface which exposed one minute at 500^{o}C Se flux and then cooled to growth temperature. When temperature reached growth temperature, firstly Zn shutter and few second later Se shutter were opened. The second growth type is that Ga-rich surface which was obtained by without Se exposure at high temperature. These growths were started with Se flux and after Zn shutter was opened. The influence of Se treatment as a function of growth temperature was examined on ZnSe layer quality by using AFM measurements. They observed that growth temperature was above 320^{o}C for Ga-rich surface, roughness was increasing. In contrast to Ga-rich surface, roughness started only above 360^{o}C for Se-rich surface Figure 7.

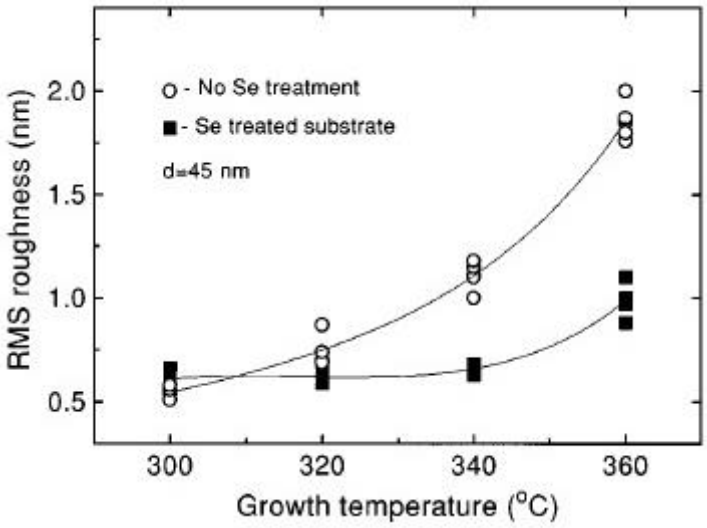

Figure 7. Surface roughness of ZnSe layer as a function of temperature with and without Se treatment [56].

Starting of growth procedure with firstly Se or Zn source is important for crystal quality of film. If the growth is started with Se source, Gallium and selenium form like Ga_2Se_3 at the interface and it badly affected crystal quality during the growth. However, when firstly Zn was sent to substrate, there was no similar reaction[58]. Therefore, Zn source was opened and after few second Se source was opened. GaAs substrate was covered initially Zn atom monolayer. By doing this, Se atoms were not compound Ga atoms.

Growth rate of ZnSe is affected by temperature and flux ratio [27]. According to K.W. Koh and his research group, decreasing of growth rate is due to the low sticking probabilities of Zn and Se atoms each other at high temperature. And also they observed that beam pressure ratio (P_{Se}/P_{Zn}) has positive effect on growth rate. Growth rate increased with increasing beam pressure ratio but it was saturated when Se to Zn ratio was started to higher.

Apart from MBE, the other growth method of ZnSe on GaAs is migration enhanced epitaxy (MEE) [59]. It is a modification technique of MBE. The difference between them is source are opened and closed respectively during growth in MEE. Migration enhanced epitaxy (MEE) was used to have good film and observe suitable critical thickness by J. M. Gaines's groups. They focused on initial exposure of Zn and Se source on GaAs substrate. They decided which one improved crystal quality and reduced strain. When firstly Zn source was sent to GaAs substrate, nearly perfect film

was obtained. Strain was compared for MBE-grown and MEE-grown which was initial growth started with Zn or Se (Figure 8). According to graph, Se-started films were more relax than Zn-started films.

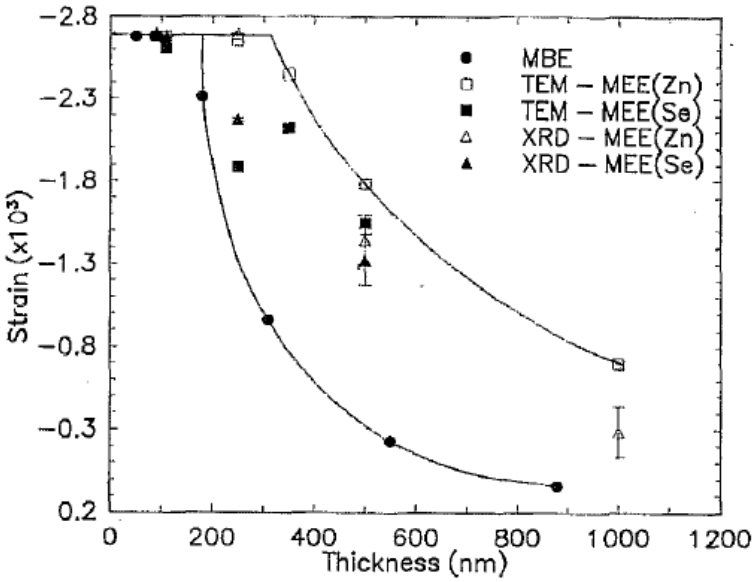

Figure 8. Strain vs. thickness of ZnSe layer for MBE-grown and MEE-grown [59].

Strain changing of ZnSe is also observed in Raman measurement. Due to the lattice mismatch, strain are happened at high temperature whereas thermal strain are happen due thermal differences at low temperature [3]. The Raman spectrum of 0.5 μm ZnSe grown on GaAs(100) is shown Figure 9 [60].

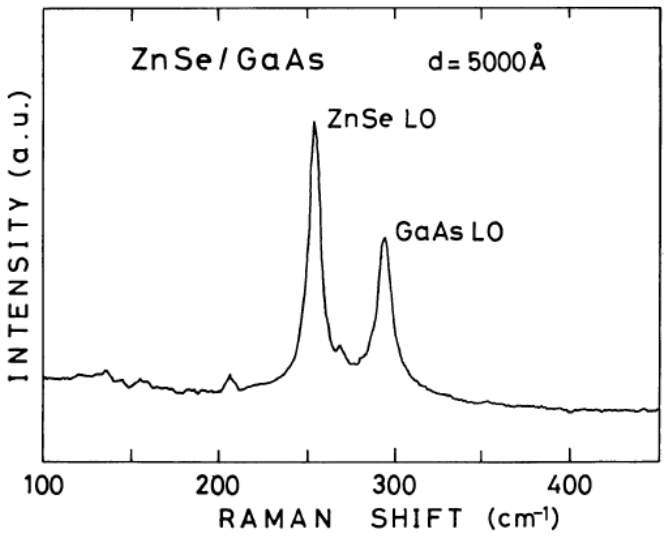

Figure 9. The raman spectrum of ZnSe on GaAs [60]

The longitudinal optical (LO) phonon frequency of film thickness was analysed and Raman shift was observed with regard to elastic strain and thermal strain at different temperature by K. Kumaza.

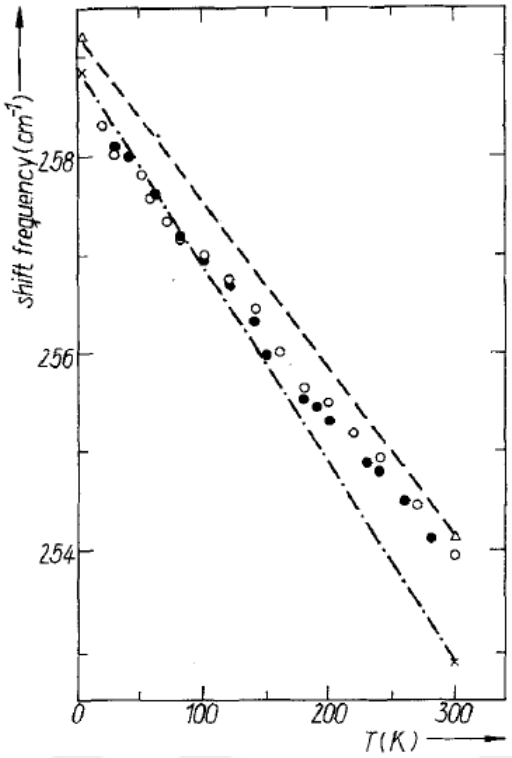

Figure 10. Raman shift frequency of MBE-ZnSe films with 0.45 (open circles) and 1.2 pm (full circles) [3].

Shift frequencies of film was nearly ± 1 cm^{-1} at low temperature and ± 0.8 cm^{-1} at room temperature [3]. Frequencies were increased with increasing temperature because the film of crystals were started softening (Figure 10).

CHAPTER 3

ZINC SELENIDE GROWTH TECHNIQUES

3.1. Epitaxial Growth Techniques

In order to growth ZnSe epilayer, there are variety of epitaxial growth methods. These are Molecular Beam Epitaxy (MBE), Metalorganic Vapour Phase Epitaxy (MOVPE), Atomic Layer Epitaxy (ALE) and Pulsed Laser Deposition (PLD).

3.1.1 Molecular Beam Epitaxy (MBE)

Molecular Beam Epitaxy (MBE) was invented in the 1970s at Bell Telephone Laboratories by Alfred Y.Cho and J.R Arthur [61]. to grow high purity and quality semiconductor film on some substrates. The meaning of epitaxy comes from Greak words. ‘Epi’ means resting above and ‘taxy’ means ordered. There are two kinds of epitaxy. First one is homoepitaxy which is film and subsrate same material. Second one is heteroepitaxy which is film and subsrate different material.

The principle of Molecular Beam Epitaxy growth is that atoms and cluster are produced by heating solid source. After they migrate and place on hot surface in an UHV environment. Thanks to the control of beam fluxes and UHV, high purity and high quality material can be grown when compared to non-UHV techniques. It has also in-situ devices such as Reflection High Energy Electron Diffraction (RHEED), Spectroscopic Ellipsometry (SE) which allow control and analysis during growth. This is the important advantage when compared to other epitaxial techniques.

MBE system consists of connected modules which are variety of vacuum, epitaxy and analysis equipment, is mounted as internally and externally. The main four components of MBE are load-lock, preparation, storage and growth chamber.

Figure 11. shows the functional diagram of typical MBE growth chamber. The growth chamber has sample holder, effusion cell, beam flow chamber, fluorescent screen, which is important for Reflection High Energy Electron Diffraction (RHEED) to take in-situ characterization. And also it consists of liquid nitrogen (LN_2) cyropanel which increases the vacuum level.

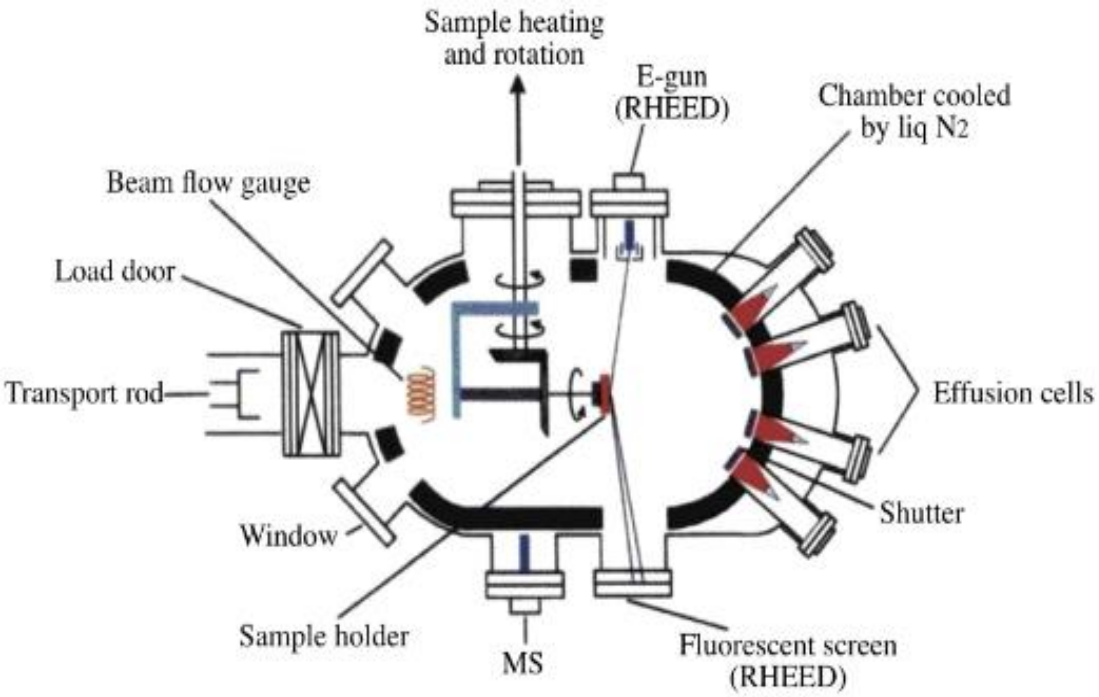

Figure 11. Functional diagram of typical MBE growth chamber [62].

Heteroepitaxial growth modes are divided into three major groups in terms of migration rates. They are Frank-Van der Merwe (FM) or layer by layer growth, Volmer-Weber (VW) or island growth and Stranski Krastanov (SK) or layer plus island growth (

Figure 12).

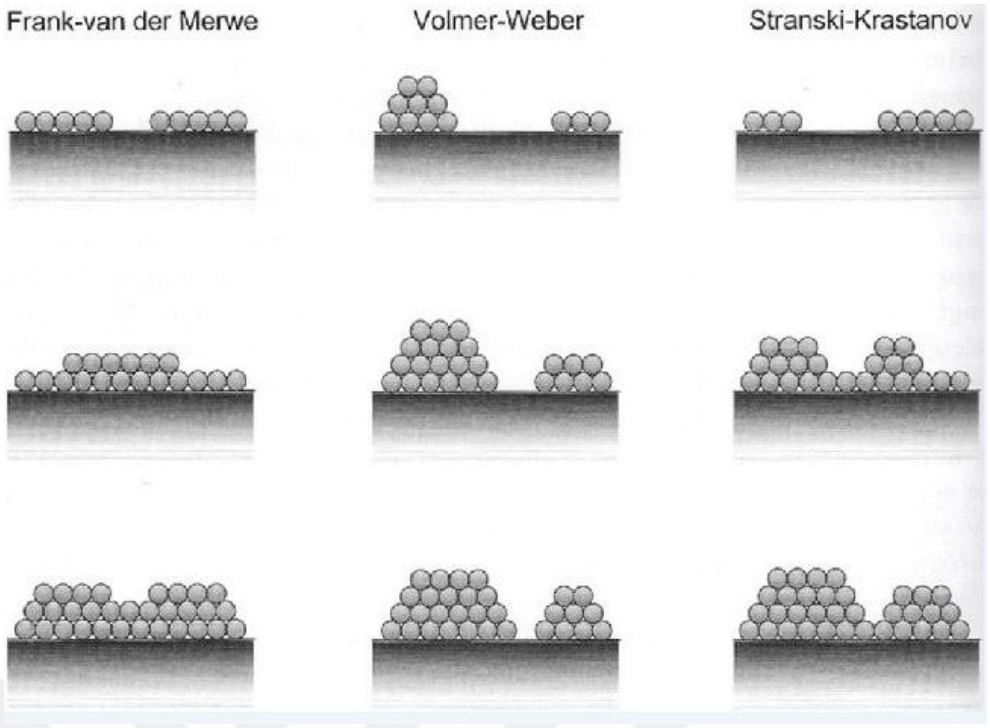

Figure 12. Growth modes of heteroepitaxial growth [63].

Frank-Van der Merwe (FM) mode is nucleated after last layer finished. It has also strong interatomic interaction between substrate and film when compared to other growth modes. Volmer-Weber (VW) can be called 3D growth. In this growth mode, atoms bound strongly in the film than substrate so islands form on the surface. Last growth mode is Stranski-Krastonov. It is as intermediate between the FV and VW. Firstly few monolayers are nucleated by FV mode and islands occur on the top surface.

The growth modes depend on some parameters. The most important are thermodynamics driving force and misfit dislocation between substrate and epitaxial layer. The growth morphology can be adopted with surface free energy of substrate (σ_s), film (σ_f) and interfacial energy (σ_i). Layer by layer growth modes happen when the sum of film and interfacial energy is smaller than substrate free energy;

$$\Delta\sigma = \sigma f + \sigma i - \sigma s \leq 0 \tag{3.1}$$

If the summation of film and interfacial energies are bigger than substrate free energy, 3D island growths happen.

$$\Delta\sigma = \sigma f + \sigma i - \sigma s \geq 0 \tag{3.2}$$

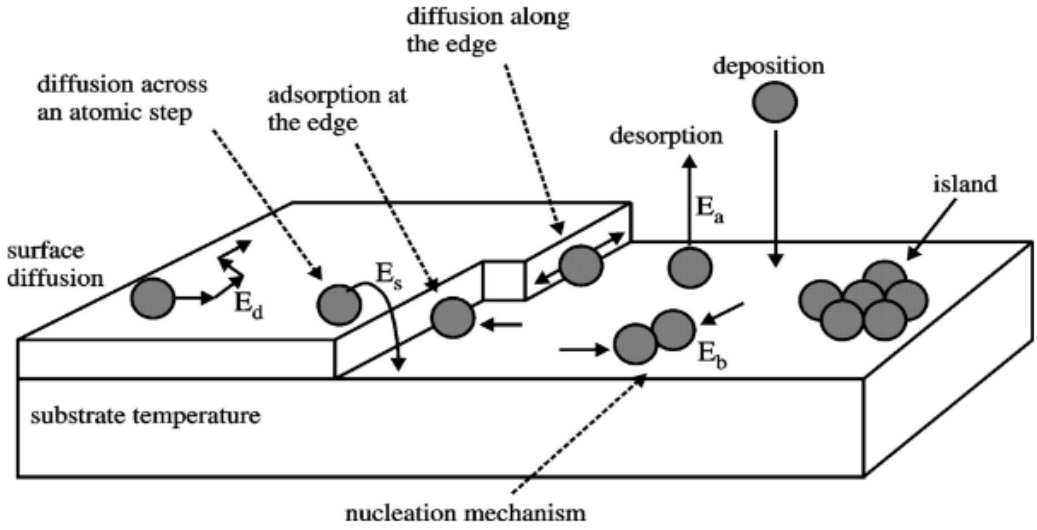

Figure 13.Atomic processes during the Molecular Beam Epitaxial growth [64].

During the film growth, some atomistic processes may be involved is shown in Figure 13. These are deposition, diffusion, aggregation of adatoms, desorption of adatomsand diffusion along step edge.

3.1.2 Metalorganic Vapour Phase Epitaxy (MOVPE)

Metalorganic Vapour Phase Epitaxy(MOVPE) was first introduced in the last 1960s to deposite semiconductor compounds from vapour phase. It is also referred like metalorganic vapour phase deposition (MOVPD) and organometallic chemical deposition [65]. The MOVPE system consists of three parts which are reactor cells, gas handling manifold and reaction chamber. The design of reactor cell is very important to obtain large-scale production. The reactor can become either the vertical reactor or horizontal reactor. These reactors are shown Figure 14. The substrate is holded on graphite subsector and then it is heated by RF coupling, resistant heater underneath the subsector. The reactor wall is cooled with water-cooled or gas cooled to reduce reaction and deposition on the surface.

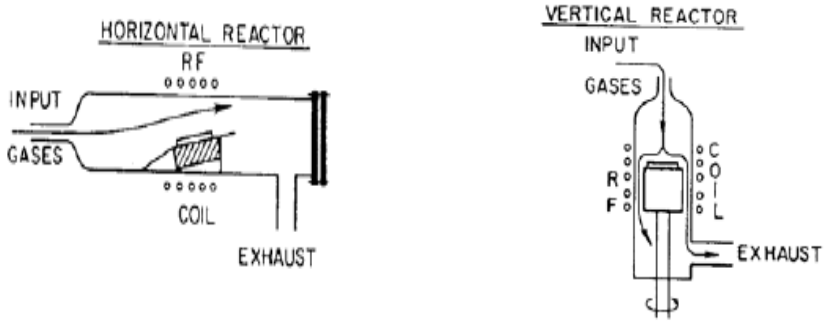

Figure 14. Schematic diagram of horizontal and vertical reactor [66].

MBE and MOVPE have advantage to obtain one monolayer on substrate with great precision. However some properties of these two epitaxial methods are different. Firstly when compared to MBE, the growth is not done at ultra-high vacuum in MOVPE. The growth are happen typically 15 to 750 torr and also used complex compound sources like metal organic sources and other gas sources [67]. Due to this gas phase, in-situ characterization equipments (RHEED and ellipsometry) are limited in MOVPE.

When compared to III-V counterparts, growth of II-VI semiconductor is carried out at low temperature by MOVPE. Growth of ZnSe can be done using ditertiarybutselenide(DTBSe) with dimethlyzinc(DMZn) at low temperature (below 400^{o}C). And also the growth depend on VI-II ratio which is VI source ratio must be greater because of high pressure of II materials. The lattice parameter of ZnSe was studied for different thickness layers grown on GaAs(100) by MOVPE with using dimethylzinc and diethlselenide. When thickness of layer thinner than 0,15 μm can grow involving strain due to lattice mismatch between ZnSe and GaAs, but thicker layers have misfit dislocations by relaxation of strain [68].

3.1.3 Atomic Layer Epitaxy (ALE)

Atomic Layer Deposition (ALD) or Atomic Layer Epitaxy (ALE) which was discovered to grow ZnS:Mn by Tuomo Suntola in 1970s is a thin film growth technique. ALE uses precursor gas while growing is performed. The precursor gas is pulsed to deposit a film on the substrate. First precursor gas is send into process chamber to produce a monolayer of gas on the surface. After that second precursor gas is send into chamber. These two precursor gas react with together and produce monolayer of film on the surface. The schematic illustration is shown in Figure 15.

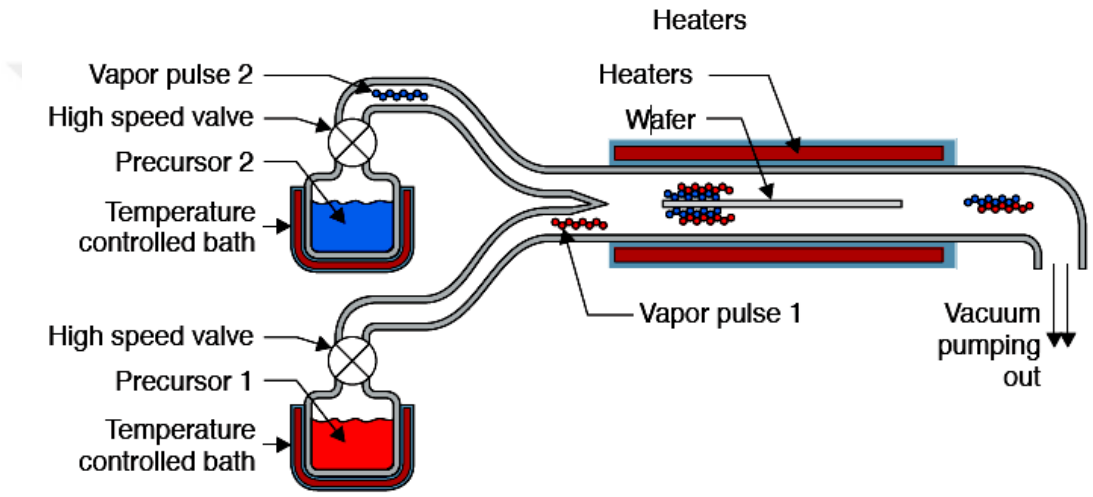

Figure 15. Schematic closed of ALD system [69].

ALE use chemical precursor like MOVPE, but growth is done under ultra-high vacuum. Thanks to these properties, in-situ characterization equipments, which enable precise control of thin film growth, are used. The wall of chamber is cooled with inert gas (N_2 or Ar) to remove unreacted precursor. The low growth rate can be said one important disadvantage of ALE. The growth rate changes between 0.5 and 1 monolayer per cycle. ZnSe was grown on GaAs (100) to observe average thickness of film per one cycle of opening and closing shutters. And also initial and successive stages were examined in detailed by using RHEED pattern [70].

3.1.4 Pulsed Laser Deposition (PLD)

Pulsed Laser Deposition (PLD) is used to obtain high quality thin film more than a decade. Firstly, it is used to grow thin film by H.M Smith and A.F Turner. The experiment was done with ruby laser, but thickness of film was not uniform [71].Until 1980's, thin film growth method was not done with PLD. Since then, pulsed laser deposition (PLD) technique has been developed rapidly and amount of research interested on this topic.

Principle of PLD is that pulses of laser are send to surface of target. When a solid or liquid is irradiated with intense laser, small of amount materials are vaporized on target and deposited to sample. It is shown schematically in Figure 16. Rotation of target holder supply homojenous growth of thin film.

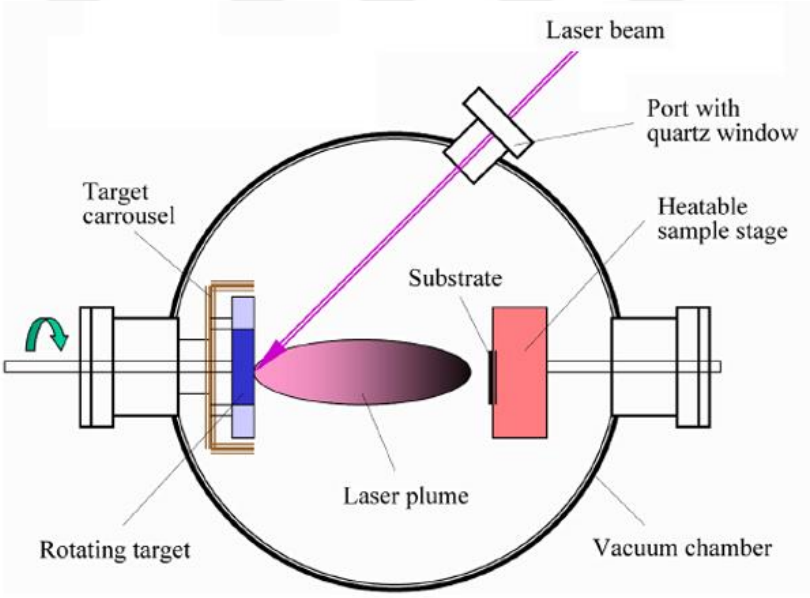

Figure 16. Schematic view of PLD [72].

This amount of vapour which is collection of atoms, molecules, ions and electrons depend on laser parameters (intensity, wavelength, pulse width). Growth is done under ultra-high vacuum so in-situ characterization is suitable for this growth method. ZnSe was grown on GaAs (001) substrate with Se and Zn target disks [73]. According to XRD and surface morphology results, ZnSe film had best crystal structure.

CHAPTER 4

EXPERIMENTAL TECHNIQUES AND PROCEDURES

4.1. MBE System Configuration

In order to have high-quality epitaxial layer which is used variety of device application, MBE system involves connected modules which are diversity of vacuum, epitaxy and analysis equipment. These equipments are mounted internally or externally. IZTECH have Gen-20MZ MBE system. It consists of three main parts which are load-lock, storage and growth (main) chambers. The functional schematic of Gen-20MZ is shown in Figure 17.

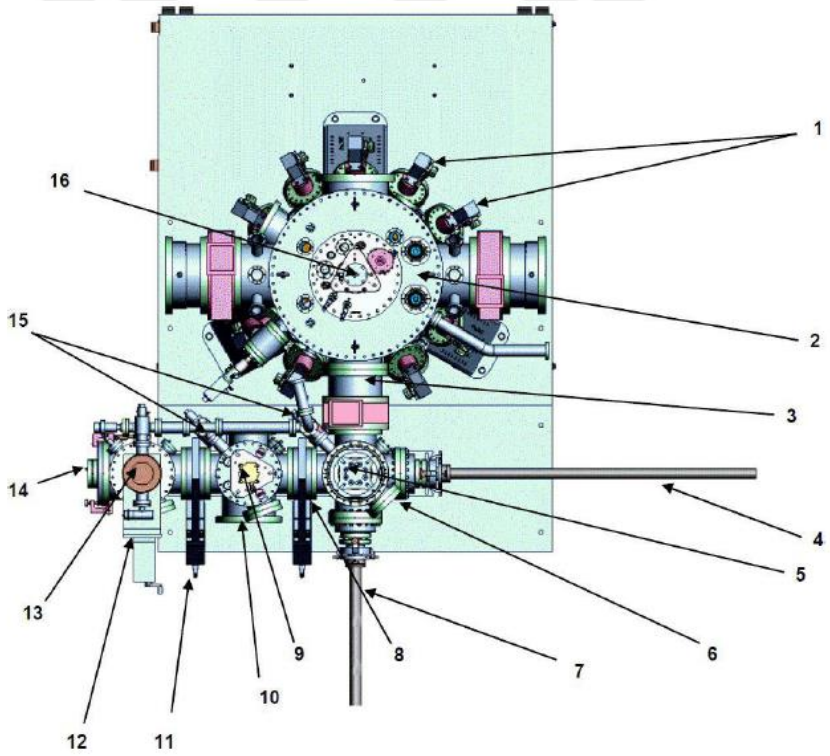

Figure 17. Schmatic diagram of Gen-20MZ. 1. Effusion cells, 2. Growth module, 3. Storage module gate valve, 4. X-axis transfer rod, 5. Storage module elevator, 6. Storage module, 7. Y-axis transfer rod, 8. Storage module gate valve, 9. Heated station for substrate outgassing, 10. Preparation module,11. Preperation module gate valve, 12. Load lock module, 13. Load lock casette elevator, 14. Load lock door, 15. Venting/roughing manifold, 16. Zaxis manipulator [74].

Firstly substrate and platens are moved into load lock module (labelled 12 in Figure 17), while the ultra-high vacuum levels of preparation chamber, storage and growth modules maintaining. Load lock has elevator-driven cassette holder. At one time, eight platens can be moved. After started in the load lock chamber, wafers are transferred to preparation chamber (labelled 11 in Figure 17) by using X-axis transfer rod (labelled 4 in Figure 17). Any residual water or contaminants is removed in the preparation chamber before wafer is transferred to growth chamber. After the outgassing is finished, the wafer is loaded to growth chamber (labelled 2 in Figure 17) by using Y-axis transfer rod (labelled 4 in Figure 17) and it is mounted Z-axis manipulator (labelled 16 in Figure 17). Thanks to Z-axis manipulator, wafer rotates and heats to obtain homogenous thickness and smooth surface while growing happen. Due to not including preparation chamber in IZTECH Gen-20MZ MBE system, oxide removal and growth process are done in the main chamber.

The growth chamber is equipped with effusion cells, cryopanel, monitoring and in-situ analysis instrument which is RHHED to characterize film during growth. And also viewports become in various location to observe substrate position before, during and after growth. L_2 cryropanels surround all main chamber wall and source flange. Thank to this any residual and particular stick on cold wall and cannot interact substrate. Also cryopanels play role like thermal isolation among different cells [75]. Band edge thermometer, pyrometer and thermocouple exist to measure substrate in the main chamber during growth. Residual gas analyser (RGA) is used to measure species of mass-to-charge (m/z) ratio and leakage tests. Effusion cells are important component of main chamber since they supply flux stability, uniformity and material purity. It consists of 12 ports each sources. The cell flux is determined by beam flux monitor (BFM). Source material obtains in effusion cell. It is heated with irradiation and temperature controlled proportional-integral-derivative (PID) controllers and thermocouple. While source material heated, effusion cells must cope with high temperature (up to 1400^{o}C) [75]. Moreover, choice of material, elements and geometry are significant. The cell geometry is important so material flux does not drift when source is depleted. The first cell was known Knudsen cell which have small orifices. It ensure thermal equilibrium between the melt and vapour in the cell. However, Langmuir type effusion cells are used in MBE growth. They have large orifice. So flux can reach with low temperature to substrate, thermal generation of impurities reduces [75].Typical effusion cell is shown schematically in Figure 18. The crucible (labelled 1 in Figure 18) is made

pyrolytic boron nitride which is tolerate up to 1300^0C. Its shape is cylindrical or conical. Source is heated by Ta filament (labelled 2 in Figure 18). Multiple Ta foils provide heat shielding (labelled 3 in Figure 18). Material temperature is measured thermocouple (labelled 4 in Figure 18). Shutter is located in front of cell and controlled with computer. Effusion cells also are applied such as arsenic and phosphorous by cracking cell because of high pressure and low sticking coefficient.

Figure 18. Schematic of effusion cell of MBE [75].

Thickness uniformity depends on molecular beam fluxes, and geometrical relation between source and substrate. The flux can be calculated below equation;

$$f = \frac{P\,a}{\pi L^2 \sqrt{2\pi m k_B T}} \; \frac{1}{s.cm^2} \tag{4.1}$$

Where T is substrate temperature (K), P is equilibrium vapour pressure of cell, "a" is the area of cell aperture, "L" is the distance between cell and substrate, "k_B" is Boltzmann's constant, "m" is mass of effusing species. And also source material molecular flux can be calculated with beam equivalent pressure (BEP) below equation;

$$BEP = I k_B T_R n \tag{4.2}$$

Where I is relative ionization, T_R is room temperature and n is molecular density.

Figure 19. Gen-20MZ MBE system in department of physics in IZTECH

4.2. X-Ray Diffraction

There are many techniques to know how atoms are arranged into crystal structures and microstructures. Diffraction experiments are useful to determine the crystal structures of materials. They give much more information about material such as revealing lattice constant, crystallographic orientation, strains and defect densities.

X-rays are produced in x-ray tube which contains two electrodes, the cathode and anode, in a vacuum evacuated. Electrons are supplied with heating filament (Figure 20). They are accelerated by large potential difference from cathode to anode. By using electric fields, electron beams are focus on anode. When they hit the tungsten anode, electrons lose energy ionization and radiative collision with target atoms. These interactions produce characteristic X-rays.

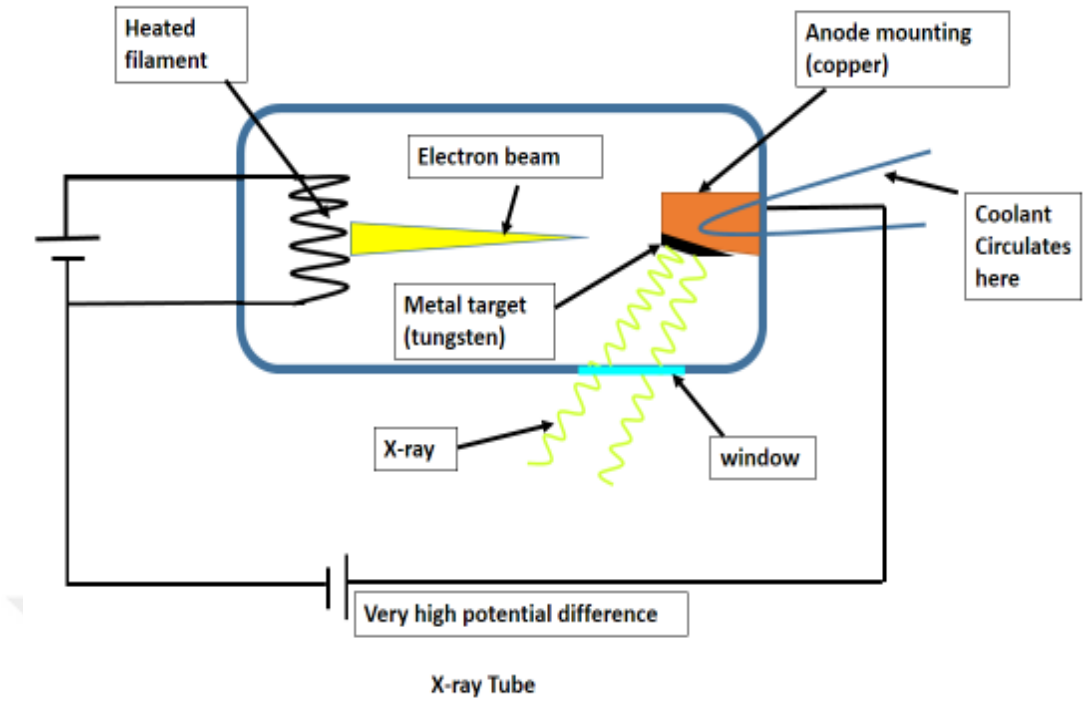

Figure 20. Basic shape of X-ray tube

In diffraction experiment, the beam of incident X-rays is directed into sample and detector records the reflected beam to obtain direction and intensities of diffracted waves. Thanks to different types and position of atoms, constructive or destructive interference happens after diffracted. This interference contain diffraction pattern which gives information about crystal structure of material. When periodicity of crystals is precise over long distance, diffraction peaks are sharp and clear. If crystals have defects, which are impurities, dislocations or small precipitates, the periodicity is less and diffraction peak are weakened, broadened and distorted. However, this is important to analyse crystal defects.

The construction is necessary to derive Bragg's law. The angle of incidence is θ and the interplanar spacing is d. The ray scattered from top plane to bottom plane. The path difference is 2dsinθ (figure2). Constructive interference occurs when difference of path length for bottom and top ray is equal to one λ.

$$2dsin\theta = \lambda \tag{4.3}$$

When the path difference is nλ between two reflected beams, constructive interference occurs.

$$2dsin\theta = n\lambda \tag{4.4}$$

All material contains many distinct peaks, they represent different interplanar spacing, d. For cubic crystals,

$$d_{hkl} = \frac{a_0}{\sqrt{h^2 + k^2 + l^2}} \tag{4.5}$$

Where a_o is lattice parameter, hkl miller indices, d_{hkl} interplanar spacing.

4.2.1 X-Ray Reflectivity

XRD measurements are used to obtain information about crystal size, lattice strain and orientation of thin film material. However, X-ray reflectivity differs from XRD. It is destructive and surface sensitive technique. XRR measurement is used to determine thin film parameters which are thickness, density and roughness of surface and interface. It can be applied to study amorphous surfaces, single crystal.

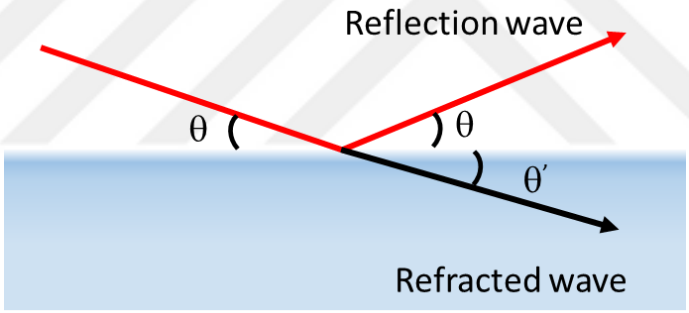

Figure 21. Reflection and refracted wave on the surface

In X-ray reflectivity, electromagnetic waves send onto a sample surface, then these incident electromagnetic waves generate reflected waves, which reflect on the surface, and some wave refract in the surface (Figure 21).

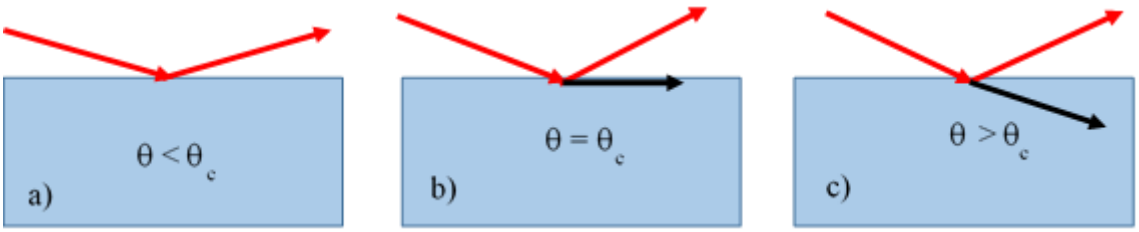

Figure 22. Reflection and refracted wave depending on incident angle

4.2.1 X-Ray Rocking Curve

X-ray double crystal rocking curve (XR-DCRC) is used to find distribution orientation of crystal in material. And also strain, lattice mismatch, relaxation etc. can be determined by using this method. Figure 23 shows basic X-ray experiment Setup. The incident angle (θ) is defined as the angle of between the X-ray source and the sample. The diffracted angle (2θ) is defined between the incident beam and the detector angle. In θ:2θ instrument the tube is fixed, the sample rotates at θ°/min and the detector rotates at 2θ°/min. In θ:θ instrument the sample is fixed and the tube rotates at a rate -θ°/min and the detector rotates at a rate of θ°/min.

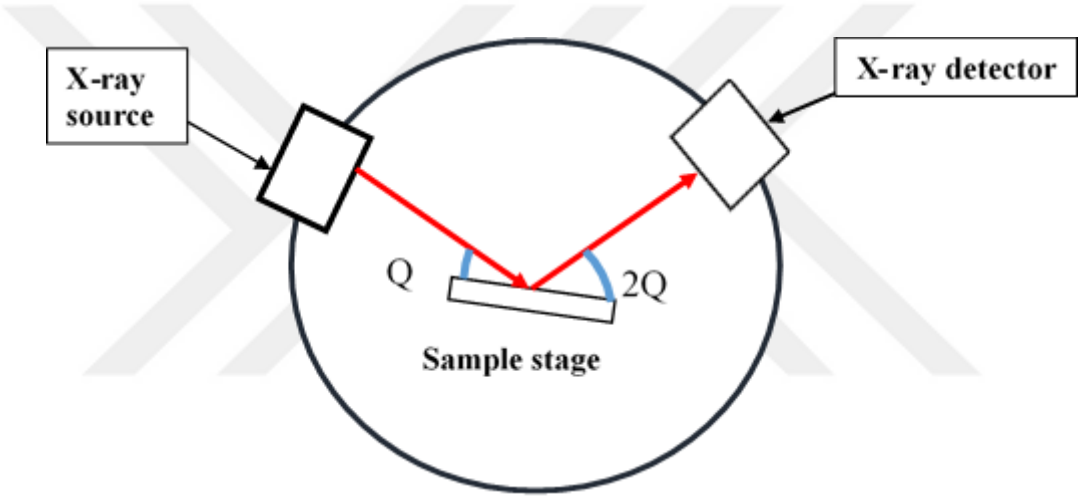

Figure 23. Basic features of a typical XRD experiment

Full width at half maximum (FWHM) value gives information about crystal quality of film Figure 24. Decreasing value of FWHM means that the film crystal quality start to improve. XR-DCRC of FWHM is measured as arcsec which is calculated by using 1^0 = 3600 arcsec.

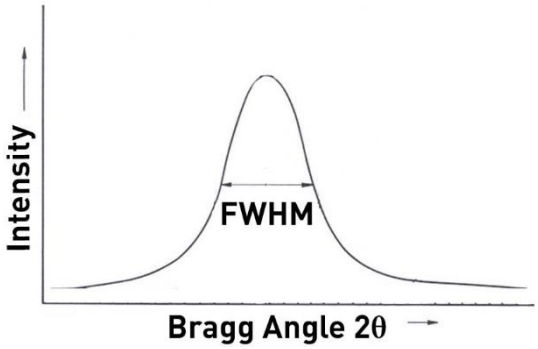

Figure 24. Schematic presentation of XR-DCRC FWHM [76].

4.3. Ellipsometry

In late 1880s, first ellipsometric studies were done by Paul Drude [77]. His studies were about absorbing and transparent solids to find optical properties of those solids. After that, very little developments were observed ellipsometry to 1945. Alexandre Rothen reported the half-shade technique. By doing this, he could detect change of polarization when light reflected from a sample. It was named 'ellipsometry'[78]. And then ellipsometers were enhanced various purpose [79]. Lastly in 1990, the real time spectroscopic ellipsometry was developed to obtain simultaneously for analysis of thin film growth and material processing [80].

The optical properties of material are found spectroscopic ellipsometry (SE). Thin film thickness can be investigated with optical models. Incident light must penetrate the film and the light reflected from interface surface to the film and lastly reach detector. Thanks to this process, film thickness measurements are done. The band gap of light spectrum must be smaller than band gap of semiconductor. Therefore light cannot be absorbed from semiconductor film and light reflected from interface. Crystal quality, area uniformity, roughness can be found by SE.

Dielectric function of sample is determined with Spectroscopic Ellipsometry (SE) by measuring polarization angles of reflected light. Psi (ψ) and Delta (Δ) are polarization angles. They are related to amplitude ratio of electric field of polarized light and phase difference light, respectively. The measured parameters ψ and Δ is important for sample. Because, these parameters give information about film thickness and optical constant of sample. And also energy bandgap, surface temperature, alloy composition are learned with optical constants which are dielectric constants or refractive index.

Data analysis is important spectroscopic ellipsometry (SE). If it is not performed, SE only can measured Psi and Delta versus wavelength. SE data must be used usually to determine properties of sample which are layer thicknesses and optical constants. The based model analysis is summarized in Figure 25. The steps can be ordered like this. Firstly SE data is measured on the sample. A layered optical model presents structure of sample. This model is fitted by software to enhance agreement between measured data and model of SE which is generated in software. Lastly the

results are compared. If the results are not compatible the optical model and fit parameters are modified again and fitted.

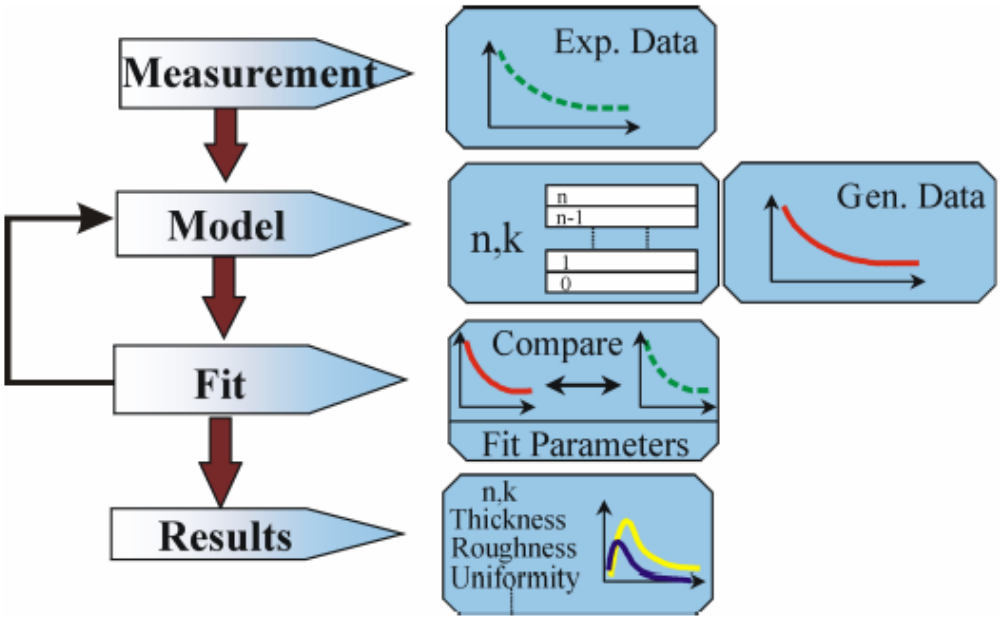

Figure 25. SE Data Analysis based model [81].

Mean squared error (MSE) define how differences between the measured data and model generated data. Correction of thickness of layer and optical parameters are decided with MSE. The value of MSE can be expressed in equation.

$$MSE = \sqrt{\frac{1}{3n-m} \sum_{i=1}^{n} [(N_{E_i} - N_{G_i})^2 + (C_{E_i} - C_{G_i})^2 + (S_{E_i} - S_{G_i})^2]} \times 1000 \qquad (4.6)$$

Where ‘n’ is the different wavelength value of incident light and ‘m’ is the number of fit parameters. N, C and S are element of isotropic Mueller Matrix. Multiplicative factor of 1000 makes ideal MSE value which is approximately 1 because 0.0001 is accuracy in experimental N, C and S. For example MSE value of thin film is expected 0.5-2 range and for more complex film such as thick film is 10-20 range. The lower MSE value means that better fit between experimental and generated SE data.

The simple type of samples of thickness can be analysed with optical constant. These thicknesses are determined in the optical model fit. However, most samples do not happen in this category, their optical constant are rarely constant. They depend on material deposition and processing condition. Example of experimental data Si with native oxide can be seen in Figure 26 as pseudo dielectric function. Optical constants

are available Si substrate and oxide layer in Woollam library [81]. These constants are shown in Figure 26 and Figure 27.

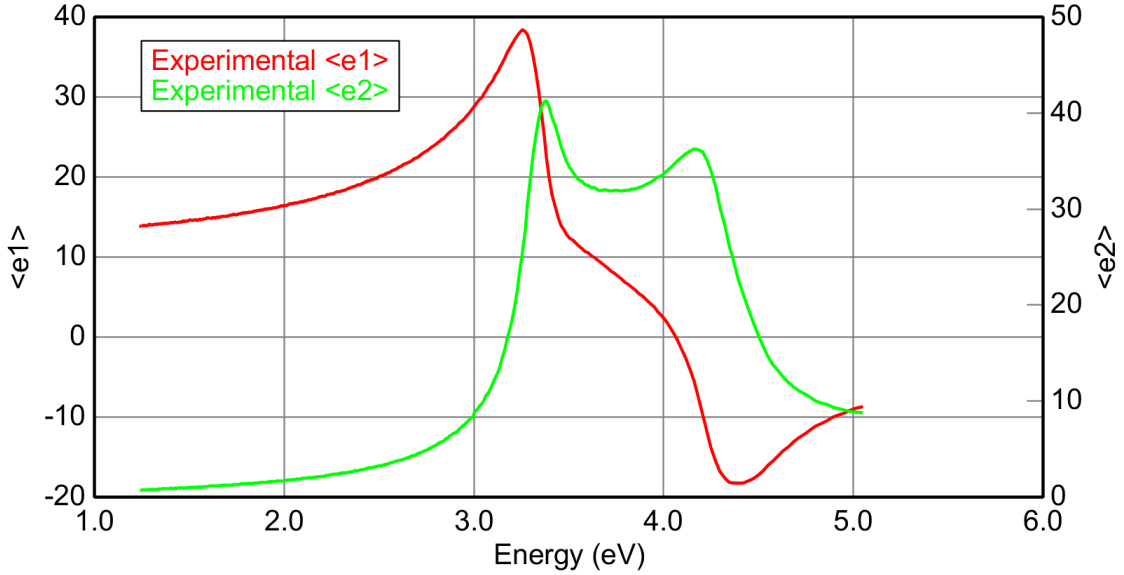

Figure 26. Experimental data of Si with native oxide as pseuda dielectric function [81].

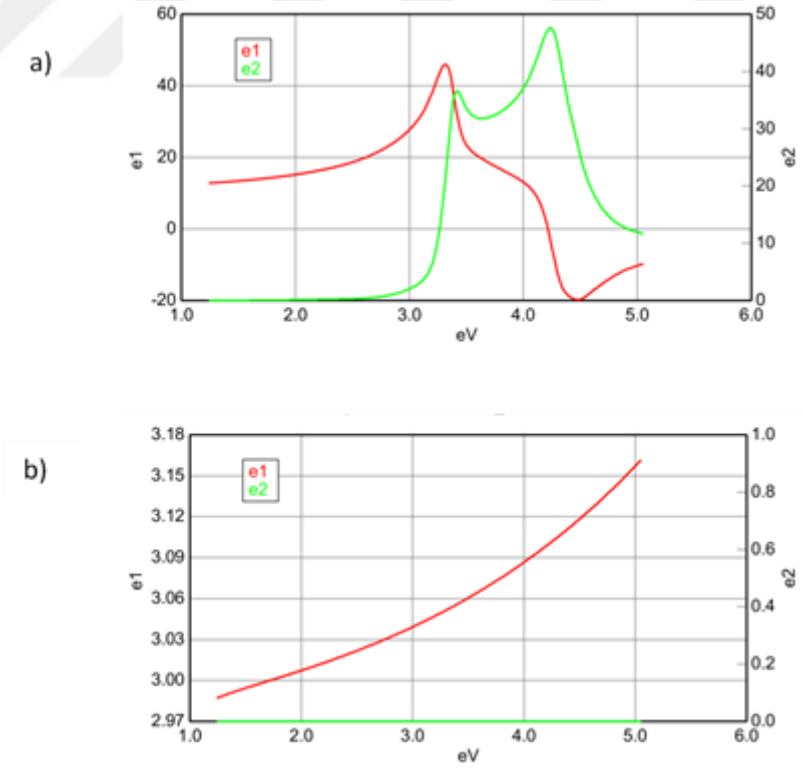

Figure 27. Optical constant of (a) Si and (b) native oxide [81].

After measurement of sample, the model is chosen in Woollam library. This model consists of Si substrate and oxide layer (Figure 28). Model data provides information about (ψ, Δ) spectral data (Figure 29). Then experimental data and model data are compared (Figure 30) to see fit degree. By using these results, oxide thickness value can be found by SE software. If the result is not suitable MSE which is not enough small, the other optical model is used.

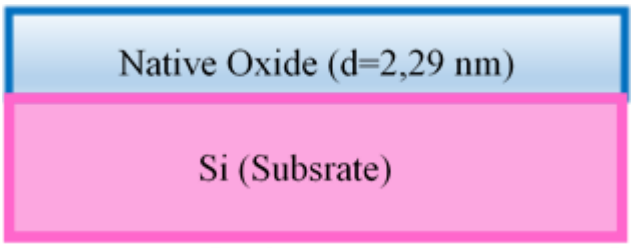

Figure 28. Si with native oxide

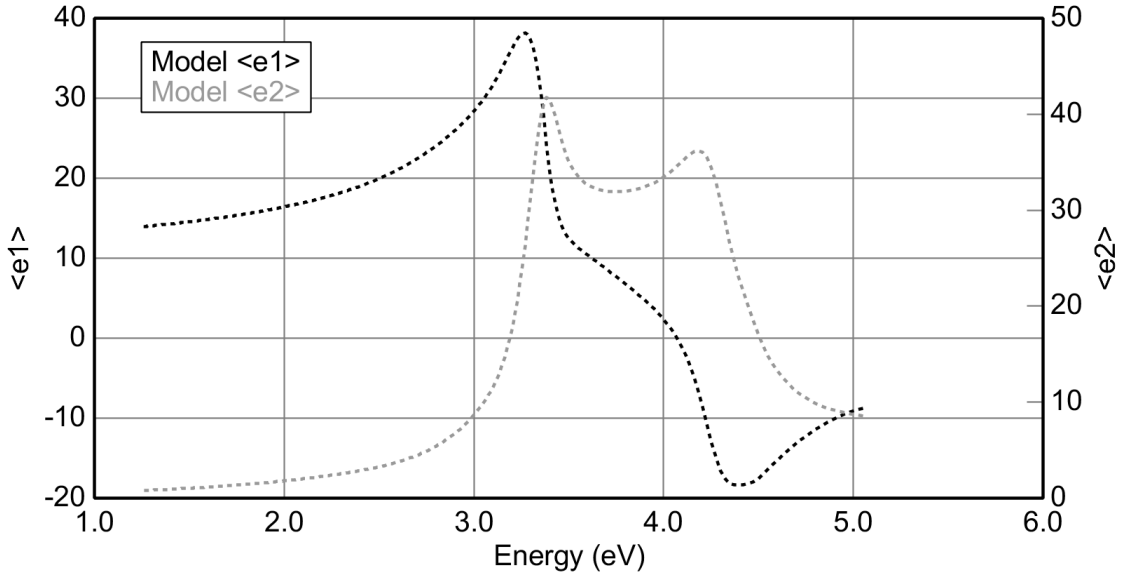

Figure 29. Model for Si substrate with native oxide

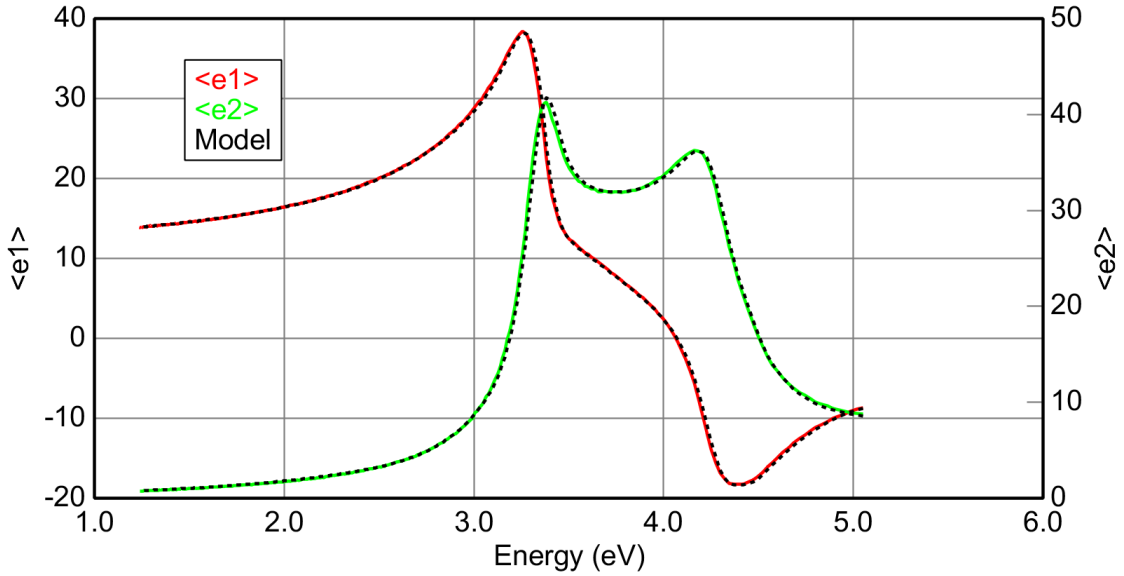

Figure 30. The correlation results between experimental and model data [81].

4.4. Atomic Force Microscopy

Binary and Quate exhibited about Atomic Force Microscopy which was main improvement in 1986. AFM is a mechanical imaging instrument that gives us information about physical properties of a surface and also three dimensional topography with sharpened probe. This small probe tip is very ultra-small and highly small interaction on area and this interaction are done with small forces. The tip is attached with a very soft spring to obtain these forces. Cantilevers are made silicon (Si) or silicon nitride (Si_3N_4) materials.

The deflection of cantilever is exactly corresponding to the tip-sample interaction force. This deflection can be obtained by using the Hooke's law:

$$F = kx \tag{4.7}$$

Where x is deflection of cantilever which is founded by dividing force with spring constant k.

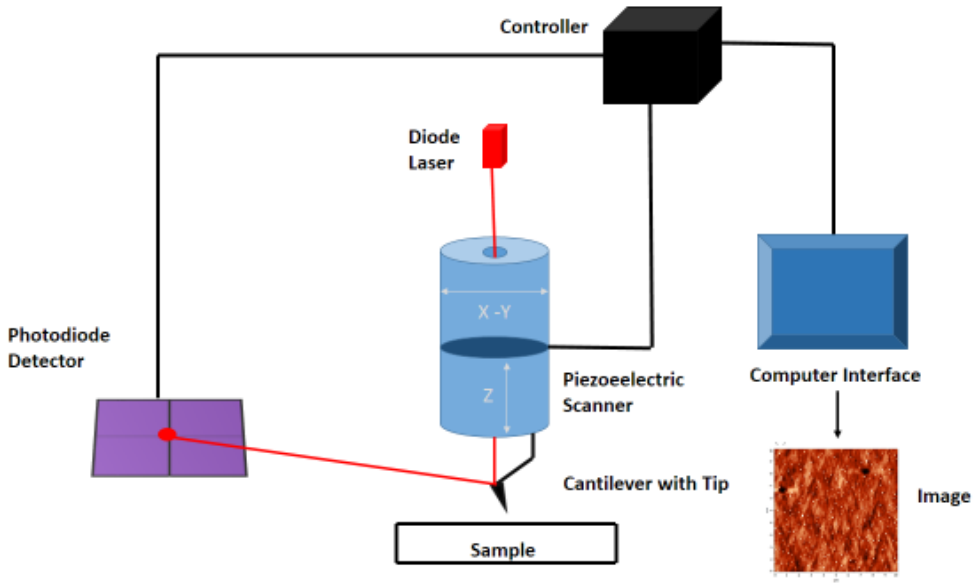

Figure 31. Schematic illustration of AFM components

A laser is reflected back of the cantilever and collected in a photodiode to detect the displacement of cantilever (Figure 31). Displacement of cantilever is detected by optical detection of AFM. Firstly a laser is reflected back of the cantilever and then the reflected beam is collected in photodiode. The photodiode is semiconductor material. It turns reflected beam into an electrical voltage signal. The diode is divided into four sections. Vertical and horizantal movements are differentiated. Vertical movement is measured the difference in voltage between upper and lower quadrants of photodiode. Horizantal movement is indicated that vertical and horizantal movements of reflected beam are differentiated on photodiode. Vertical movement is measured difference of voltage between upper and lower quadrants of photodiode. Horizantal movement is likely measured diffrence of voltage between left and right quadrants of photodiode.

Feedback control is important in AFM to maintain fixed force between the probe and the surface. Thanks to feedback mode, correct position of probe and surface are established. The Lennard-Jones potential identifies the relationship between the tip and sample interaction forces. It depends on tip and sample surface distance. The potential energy of two atoms is given by;

$$U(r) = 4\varepsilon\left\{\left(\frac{\sigma}{r}\right)^{12} - \left(\frac{\sigma}{r}\right)^{6}\right\} \tag{4.8}$$

Where ε is constant and measure how two particles attract each other. σ is the distance between two particles at which intermolecular potential is equal to zero. σ gives information about the distance between close two nonbonding particles and is referred as van der Waals radius. Distance between tip and sample depend on Van Der Waals force which is shown in Figure 32.

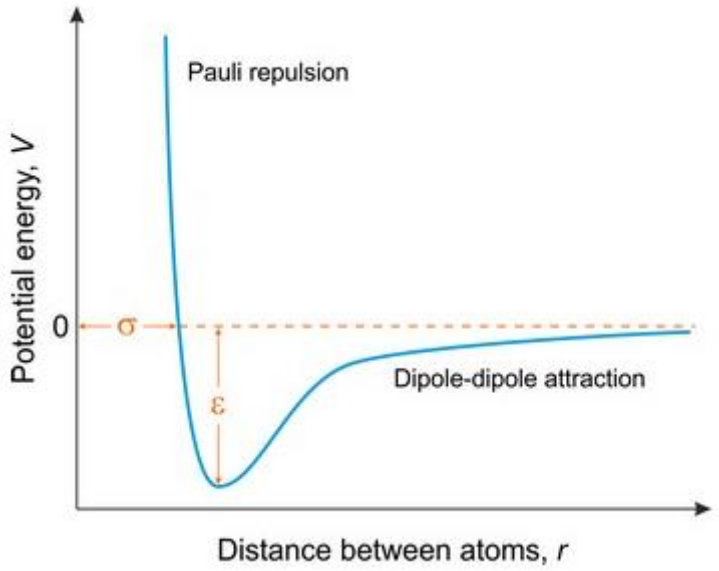

Figure 32. Lennard-Jones potential [82].

There are three types AFM imaging modes. They are contact mode, tapping (semi-contact) mode and non-contact mode (Figure 33).

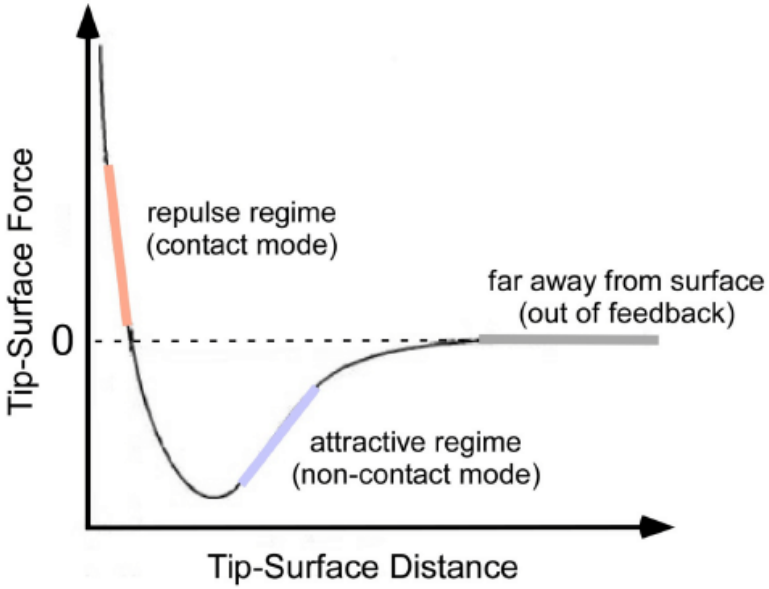

Figure 33. Potential energy diagram of a probe and sample [83].

4.5. Nomarski Microscopy

Nomarski is used diffraction interference contrast, DIC. The images are taken like three-dimensional with shadow and relief appearance. Polarized light is used while the image is taken.

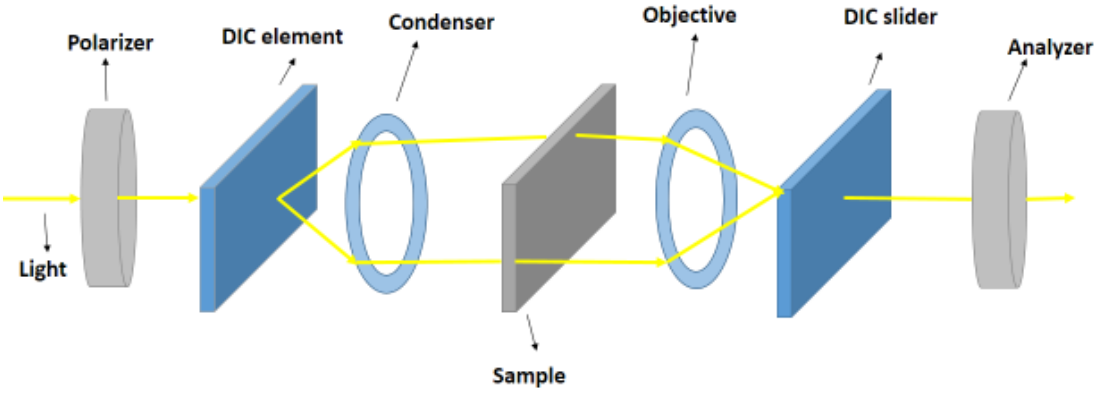

Figure 34. Schematic diagram of Nomarski microscope

The working principle of Nomarski is shown in Figure 34. There are two DIC prism. First one is placed behind the polarizer and in front of the condenser lens. Second one is placed behind objective lens and in front of the analyzer. Two beams are created by using first prism. This first DIC prism divides the polarized light beam with polarizer. Two parallel beams travel along different paths. If the sample does not achieve a path difference between two parallel beams, the second DIC prism rejoins the pairs and produces linearly polarized line. It is the same as before line which was split by first DIC prism. Therefore, analyzer will close light transmission with polarizer. However, if the sample achieves a path difference in the pair of beams, rejoined is produced by the second DIC. It will be elliptically polarized light. Thus the analyzer can have bright area which will be visible[84].

4.6. Raman Spectroscopy

Raman scattering or Raman effect was discovered in 1928 by Indian physicist C.V Raman who won Nobel prize in 1931. This spectroscopic technique based on inelastic scattering of monochromatic light and usually laser source is used. Inelastic scattering means that the energy of incident and scattering light are different. The monochromatic light changes when it interacts with sample. Frequency of scattered light is shifted up or down respect to original monochromatic frequency. It is called Raman effect.

The energy difference between the incident and scattered light cause the frequency shift $\Delta\nu$. It is shown Figure 35.

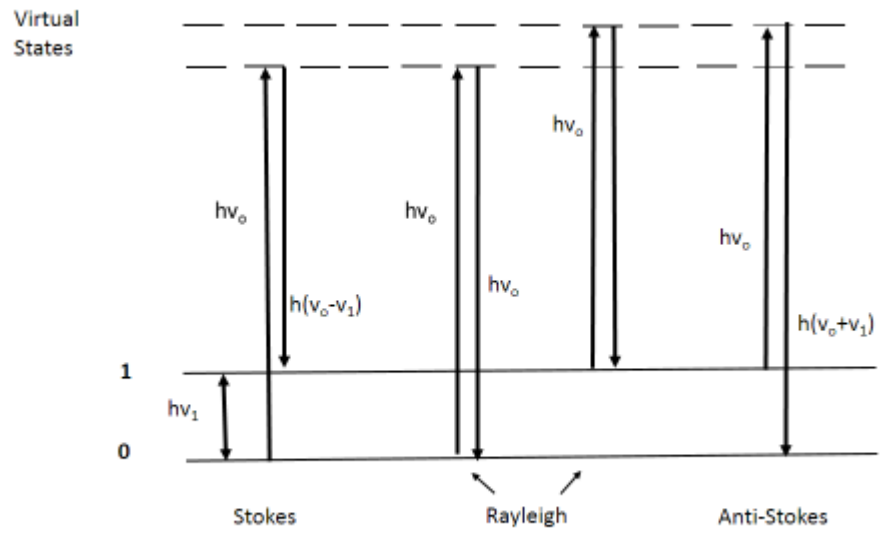

Figure 35. Raman and Rayleigh Scattering of Light

Most of molecules are firstly in the ground state (label 0 in the Figure 35) but some of them will be in excited state due to thermal agitation. When the scattering process starts, incoming photons raise to a virtual excited state. It must fall back to lower state because the molecule does not have enough energy to remain in virtual state. If the molecules find same level which is started, there is no frequency shift and we have Rayleigh scattering. But, if the molecule falls into different level, the emitted of photon energy is different from incident photon. By doing this, total energy is conserved. The frequency of incident photon (ν_o) is absorbed by Raman-active

molecule. Part of photon energy is transferred to Raman-active mode. As a result, frequency of scattered light is reduced. It is called Stokes line. The photon can also gain energy from the molecule. Thank to this, the frequency of scattered light increased. It is called Anti-stokes line [85].

Laser beams are supported by laser source. The objective focuses the light over the sample. Light is scattered on the sample. After that this light pass optical path to reach a detector. The data analysis is done by computer program (Figure 36).

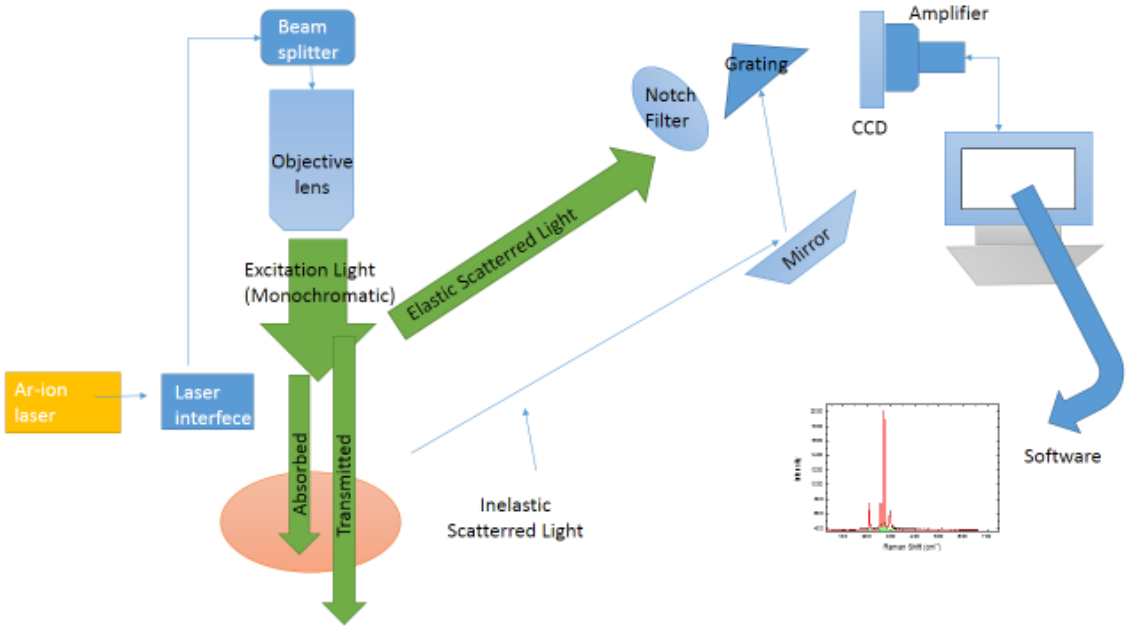

Figure 36. Schematic representation of Raman spectroscopy

CHAPTER 5

EXPERIMENTAL RESULTS AND DISCUSSION

5.1. ZnSe/GaAs(211)B Growth by MBE

ZnSe epilayer were grown on epi-ready GaAs(211)B substrate by Veeco GEN20MZ. GaAs protective oxide was removed with In flux during four minute at approximately 520-525 ^{o}C. After finished deoxidation process, temperature was increased to 545^{o}C to desorb In on GaAs substrate. Finally, the substrate temperature was cooled to growth temperature (~300^{o}C) with and without As_4 flux. When the temperature reached growth temperature, growth was carried on 120 min. Before the growth was started, Zn was sent a few seconds (~15s) on the surface to prevent Ga_2Se_3 compound. In this studies, deoxidation, flux ratio and growth temperature parameters were studied.

The temperature of substrate and molecular epitaxially grown thin film were controlled by using non-contact thermocouple measurement system. Apart from thermocouple, temperature also was measured with band edge thermometry (Bandit) and pyrometer system. Working principle of Bandit is that emitted radiation is detected from substrate. Therefore, Bandit measurement were more precise than thermocouple reading values [86].

VI/II flux ratio means rate between amount of Se which is VI group element and amount of Zn which is II group element in periodic table. VI/II flux ratio is measured by beam equivalent pressure (BEP) of Zn and Se flux during growth with looking pressure of MBE growth chamber.

The experiments were done in four parts. Firstly native oxide of substrate was removed with In flux, it took approximately 3 minutes. After that temperature was increased to desorb Indium on the substrate. Then growth was started with different flux ratio when temperature reached growth temperature (

Table **4**).

Table 4. ZnSe grown on GaAs(211)B with In deoxidation

Sample No	VI/II	Deoxidation (with In)		Desorption		Growth		
		T(°C)	Time (min.)	T(°C)	Time (min.)	T(°C)	Time (min.)	Growth rate (µm/h)
ZS1	1,7	532	3	555	3	276	120	0,18
ZS2	1,88	529	3	554	3	278	120	0,205
ZS4	3,28	533	3	555	3	303	120	0,22
ZS5	4,9	528	3	553	3	300	120	-
ZS6	4	521	3	546	3	302	120	-
ZS7	4,5	522	3	545	3	303	120	-
ZS8	5	520	3	544	3	303	120	-

In second part, deoxidation and desorption process was same as first part. The difference between them is that after desorption finished, As send to substrate to complete As deficiency. Growth parameters are shown in Table 5.

Table 5. ZnSe grown on GaAs(211)B with In deoxidation and after As sending on substrate

Sample No	VI/II	Deoxidation (with In)		Desorption		As Open T(°C)	As Close T(°C)	Growth		
		T(°C)	Time (min.)	T(°C)	Time (min.)			T(°C)	Time (min.)	Growth rate (µm/h)
ZS9	3	522	3	547	3	547	394	303	120	1,2
ZS10	2	524	3	548	3	548	400	301	120	0,972
ZS11	4	525	3	550	3	550	393	300	120	1,241
ZS12	3	524	3	550	3	549	400	300	120	0,324
ZS13	3	525	3	550	3	-	-	300	120	0,302
ZS29	2,74	525	4	548	3	548	440	300	120	0,265
ZS30	2,74	525	4	548	3	548	440	290	120	0,318
ZS31	3,1	525	4	548	3	548	440	300	120	0,306
ZS32	4	525	4	548	3	548	440	300	120	0,337

In part three, As was send before and after dexoidation process and also deoxidation was done with As flux (Table 6).

Table 6. ZnSe grown on GaAs(211)B with As deoxidation

Sample No	VI/II	As Open T(°C)	Deoxidation (with As)		As Close T(°C)	Growth		
			T(°C)	Time (min.)		T(°C)	Time (min.)	Growth rate (µm/h)
ZS14	2,74	291	606	4	423	298	180	0,336
ZS15	3	292	606	4	424	298	180	0,398
ZS16	3	290	605	4	425	272	180	0,430
ZS17	4	290	603	4	422	275	180	0,509

In the last part, As was send to substrate before deoxidation. In flux was used to remove oxide on the substrate at deoxidation process. After the desorption, As cell was open and closed at different temperature for each group (Table 7).

Table 7. ZnSe grown on GaAs(211)B with In deoxidation and before – after As sending

Sample No	VI/II	As Open T(°C)	As Close T(°C)	Deoxidation (with In)		Desorption		As Open T(°C)	As Close T(°C)	Growth		
				T(°C)	Time (min.)	T(°C)	Time (min.)			T(°C)	Time (min.)	Growth rate (µm/h)
ZS19	2,74	292	520	520	4	547	3	-	-	300	120	0,277
ZS20	2,74	293	527	527	4	547	3	547	490	302	120	0,279
ZS21	2,74	293	526	526	4	549	3	549	470	303	120	0,239
ZS22	2,74	292	524	524	4	547	3	547	450	302	120	0,270
ZS23	2,74	293	524	524	4	547	3	547	430	300	120	0,277
ZS24	2,74	293	524	524	4	548	3	547	410	302	120	0,27
ZS26	2,74	293	524	524	4	547	3	547	470	285	120	0,321
ZS27	2,74	293	524	524	4	548	3	548	470	275	120	0,358

5.2. XRD Results

To obtain crystal quality of ZnSe (211)B samples, single rocking curve (RC) measurements were taken by using Philip X'Pert PRO MRD XRD system. The X-Ray radiation which was 1.5418 Å wavelength was emitted from copper x-ray source. Table 8 shows FWHM result of ZnSe (211)B film. These epitaxial films were grown at constant temperature (~300°C) and flux ratio was changed between 3,28 and 5. By doing this, the effect of flux ratio was investigated on crystal quality. It has been seen that FWHM of ZS4 is smaller than the other samples. In Figure 37 the rocking curves of the ZnSe/GaAs heterostructures of different flux ratio was shown. When the FWHM become small, crystal quality of film start to improve and few strain and tilted happen between film and substrate (Figure 38).

Table 8. XRD characterization results of ZnSe films grown with In deoxidation

Sample No	VI/II	Growth Temperature (°C)	XRD-FWHM (arc-sec)
ZS4	3,28	303	297,43
ZS6	4	302	364,716
ZS7	4,5	303	355,21
ZS8	5	303	360

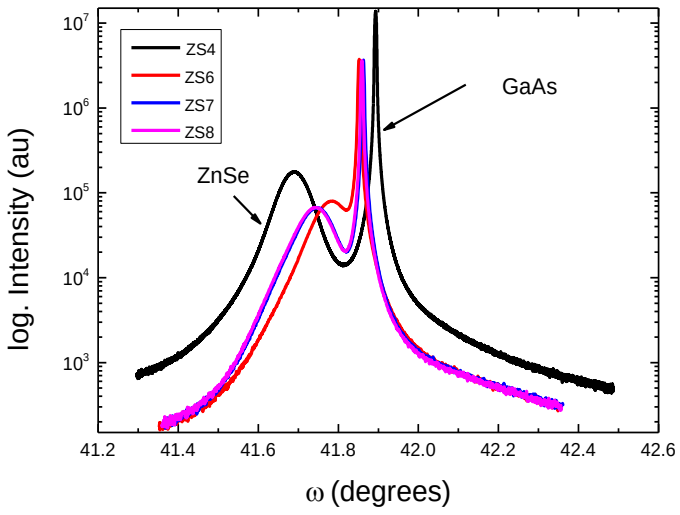

Figure 37. The rocking curve results of ZS4, ZS6, ZS7, ZS8 of different flux ratio

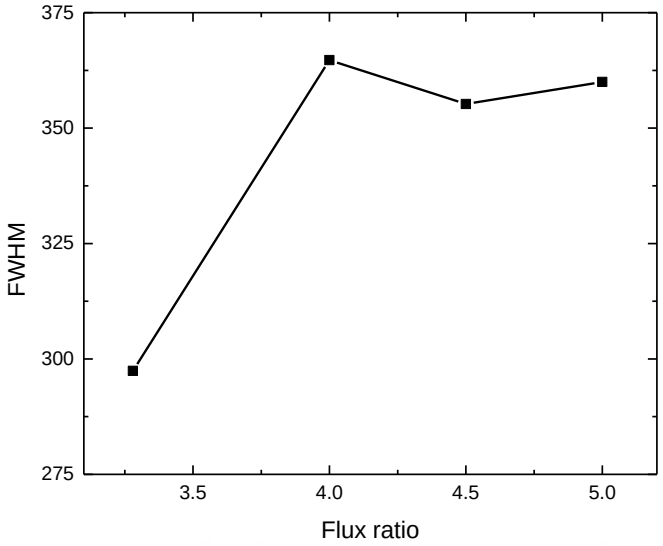

Figure 38. X-ray Rocking curve of FWHM dependence on flux ratio at constant growth temperature

While the deoxidation was being done, some As atoms were removed from the surface. We thought that lack of As may affect the crystal so As flux was send on the surface after deoxidation process was finished.

Table 9. XRD characterization results of ZnSe films grown with In deoxidation and As sending on Substrate

Sample No	**VI/II**	**Growth Temperature (^{o}C)**	**XRD-FWHM (arc-sec)**
ZS10	2	301	590,76
ZS11	4	300	550,08
ZS12	3	300	368,28
ZS13	3	300	334,26

The samples were grown same temperature (~300^{o}C), the flux ratio (VI/II) was changed between 2 and 4 (Table 9). After oxide layer was removed with In on GaAs(211)B substrate and finished In desorbtion, As flux was send at 547 ^{o}C and closed at 400 ^{o}C. The crystal quality was improved when the flux ratio was 3. In Figure 39, the rocking curves of the ZnSe/GaAs heterostructures with and without As flux was shown. ZS13 had same growth parameter with ZS12 but As was not send after deoxidation process finished, while ZS13 grown. We saw that the quality was better in ZS13 than

ZS12 which showed in Figure 40.Thanks to this result, it can be said that As does not improved sufficiently the crystal quality of epitaxial grown ZnSe (211)B.

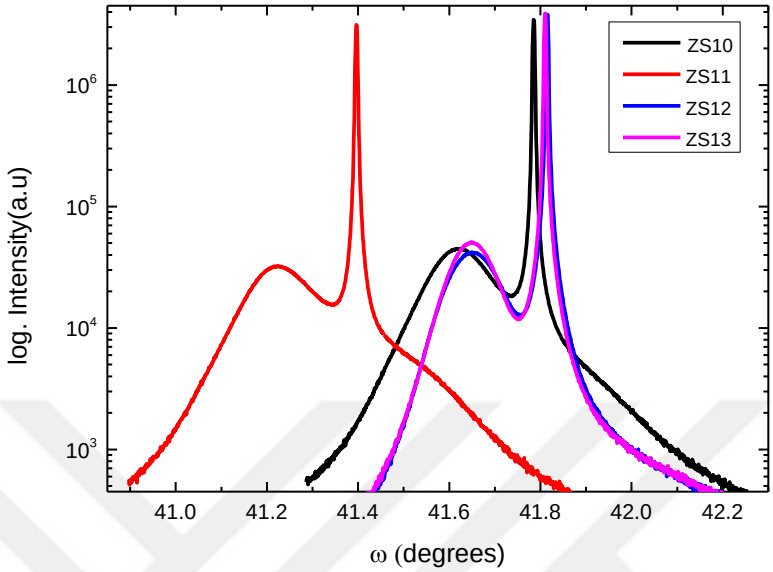

Figure 39. The rocking curve results of ZS10, ZS11, ZS12, ZS13

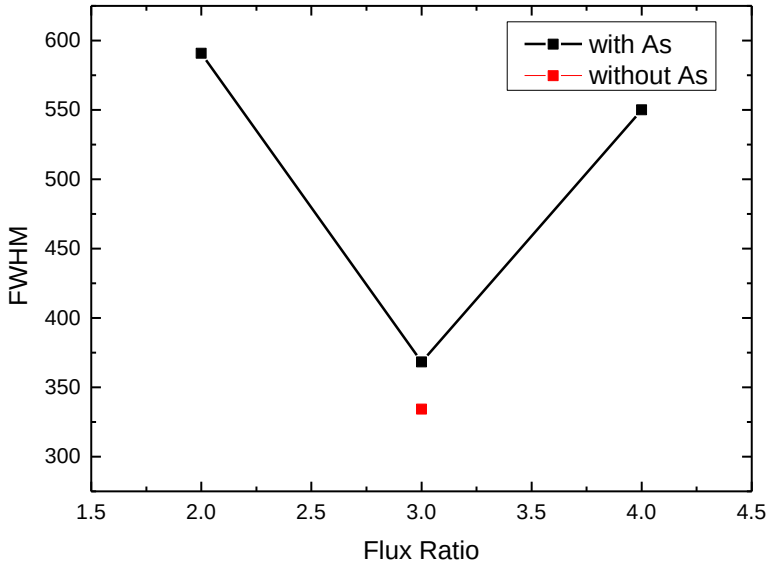

Figure 40. X-ray Rocking curve of FWHM dependence on flux ratio with and without As sending

Lastly, the oxide on the substrate were removed by using As flux. The film was grown at high and low temperature with different flux ratio. The FWHM results are seen in Table 10. ZS15 and ZS16 were grown with same flux ratio but different temperature. In Figure 41, the rocking curves of the ZnSe/GaAs heterostructures, were grown at low and high temperature, was shown.

Table 10. XRD characterization results of ZnSe films grown with As deoxidation

Sample No	VI/II	Growth Temperature (°C)	XRD-FWHM (arc-sec)
ZS15	3	298	451,44
ZS16	3	272	528,12
ZS17	4	275	626,04

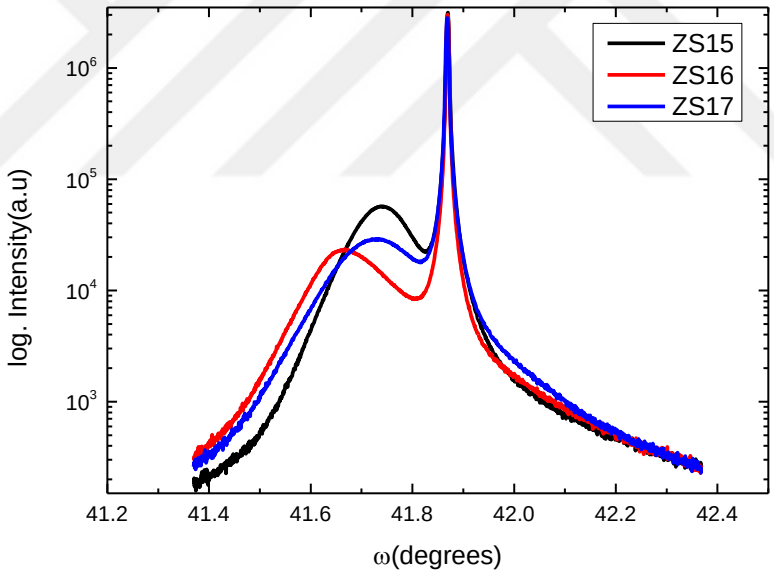

Figure 41. The rocking curve results of ZS15, ZS16, ZS17

At the high temperature FWHM of thin film was small when compared low temperature (Figure 42). ZS16 and ZS17 were grown low temperature but different flux ratio were used. The FWHM increased when flux ratio was increased.

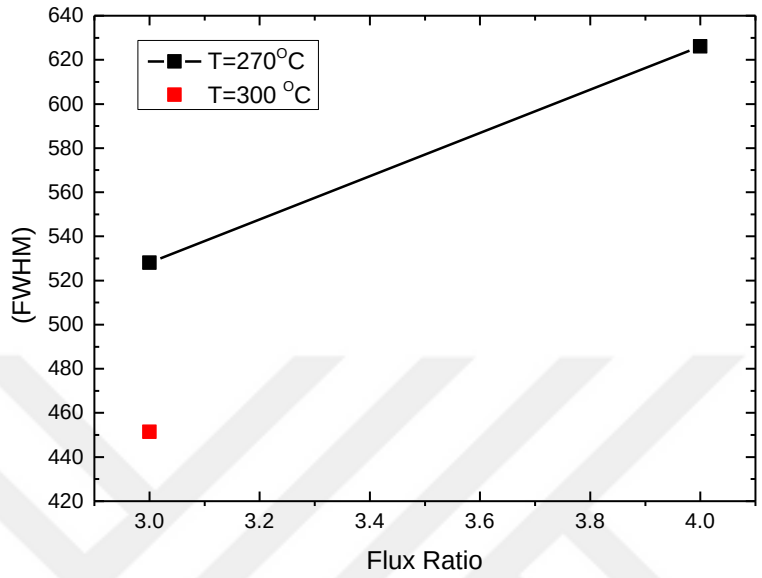

Figure 42. X-ray Rocking curve of FWHM dependence on flux ratio with As deoxdation

5.3. AFM Results

Surface quality of films were investigated with obtaining the surface root mean squared (RMS) roughness, substrate or surface defects and step-terrace structure which happened because of (211) crystal orientation, by using AFM topographical images of ZnSe/GaAs(211)B. These images were taken in semi-contact mode by Solver-Pro 7 System.

Topographic images of ZnSe films were obtained from 10×10 μm^2 area. The average RMS roughness was calculated for each sample by scanning three different region. In

Figure 43, AFM 2D images are shown for ZS4 and ZS7. The average roughness of ZS4 was found 2,3 nm. These values increased with increasing VI/II flux ratio (Figure 44), the samples were grown at 300^0C

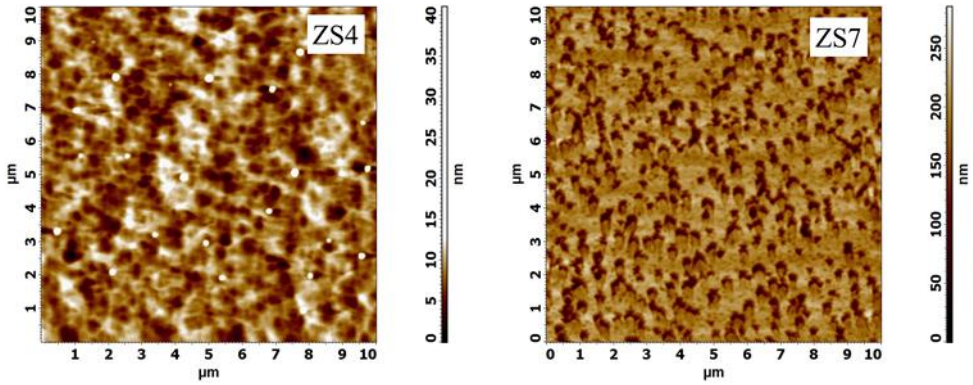

Figure 43. The AFM 2D topographical images of ZS4 and ZS7

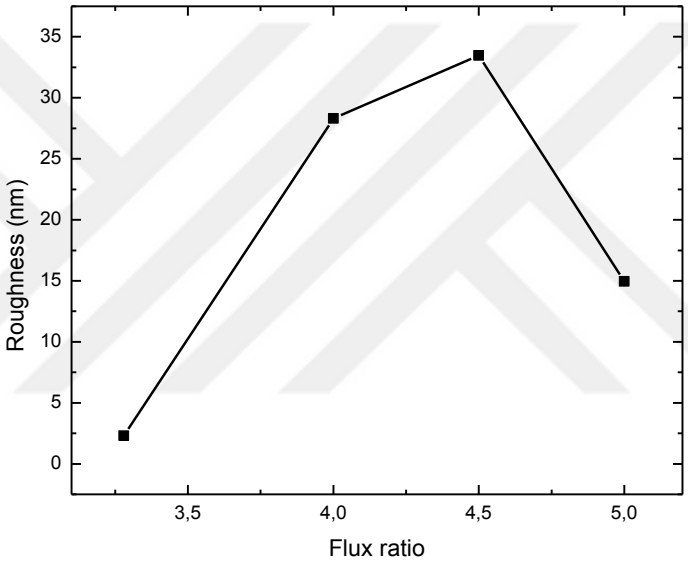

Figure 44. The Roughness depend on flux ratio

The effect of As flux and VI/II ratio change were studied on ZS10, ZS11 and ZS12. The surface images are shown in Figure 45. Firstly the roughness was increased when the flux ratio was changed from two and three. However VI/II ratio became bigger than three, RMS started to decrease (Figure 46).

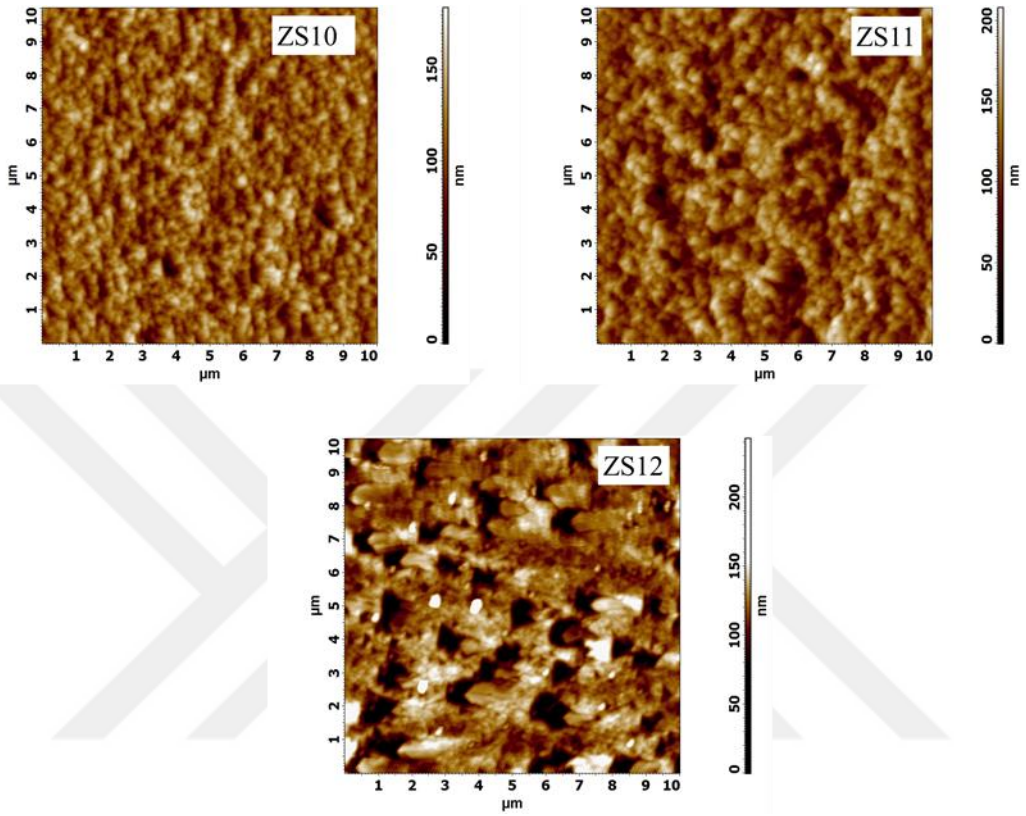

Figure 45. The AFM 2D topographical images of ZS10, ZS11 and ZS12

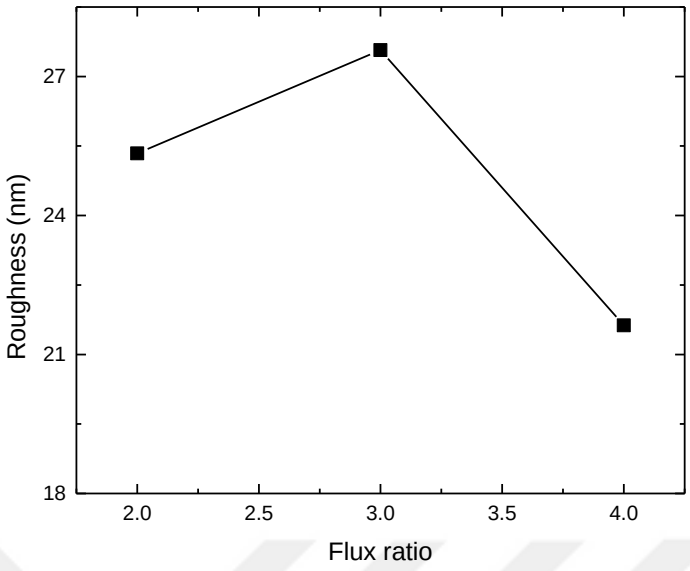

Figure 46. The Roughness depend on flux ratio

ZS12 and ZS13 were grown with 3 flux ratio at 300^0C. The differences between these samples is As was send to ZS13 after deoxidation. The RMS was found 27.57 and 16.39 nm for ZS12 and 13, respectively Figure 47. It can be seen that As reduces the surface quality of grown ZnSe films.

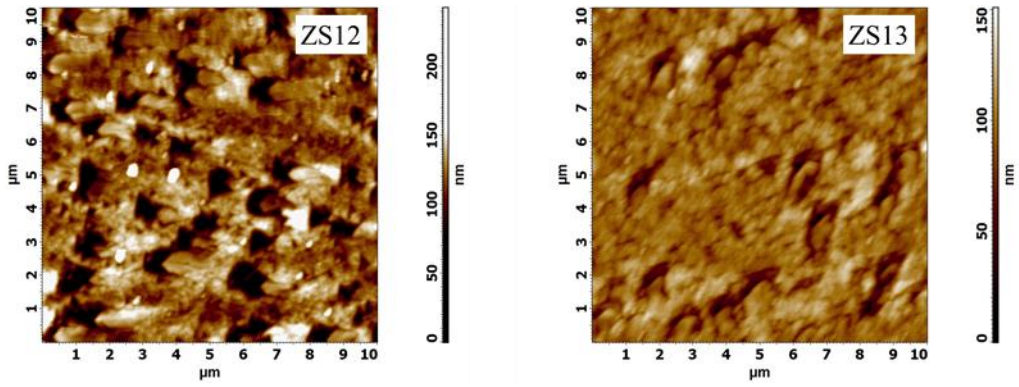

Figure 47. The AFM 2D topographical images of ZS12 and ZS13

5.4. Nomarski Results

The surface morphologies of as-grown ZnSe thin films were also detected by using Nomarski microscopy, which is A13.1013 BF/DF DIC Metallurgical Microscope, with 100x objective focus. Thanks to these analysis method, some surface defects of on ZnSe epilayer can be seen. Pyramidal structure type defects (type I) and the ridge-type defects (type II) are in two type defects[87]. These defects were observed the samples depending on growth temperature and flux ratio (VI/II).

ZS1 and ZS2 were grown with 1,7 and 1,8 flux ratio at low temperature (~275^{0}C) and ZS4 was grown with 3,2 flux ratio at high temperature (~300 ^{0}C). The native oxide of GaAs substrates were removed In flux at 530 ^{0}C and after that the temperature was reduced to growth temperature. In Figure 48, surface morphologies of ZnSe epitaxial films are seen. ZS1 and ZS2 have small defects, can be named Type- II, on the their surface. Due to the misfit dislocation or stacking faults, these defects can be produced. When the growth temperature and flux ratio were increased, defect density starts to decrease in ZS4.

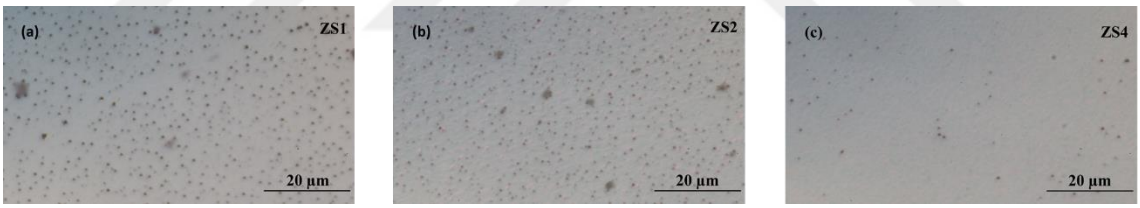

Figure 48.Nomarski microscopy images of (a) ZS1, (b) ZS2 and (c) ZS4

Figure 49 shows the effect of As flux on the surface. Flux ratio of this two samples were same which was 3. The difference was that As was not send on ZS13 after deoxidation. The shape of defects resembles pyramidal structure type defects. It can be seen that surface defects started to reduce when As was not send to surface after desorption process.

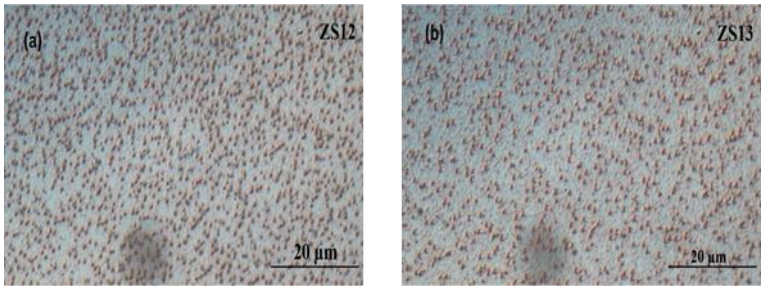

Figure 49. Nomarski microscopy images of (a) ZS12 and (b) ZS13

ZS15 and ZS16 were grown same flux ratio, which was 3, but they were grown different temperature and also these epitaxial layers were grown on 3'' GaAs(211)B wafers. The defects are more than the other sample which were grown on 20×20 GaAs(211)B wafers. It can be produced by chemisorption rate of Zn and Se atoms due to changing of substrate size. When we compared between two of them, the surface quality was start to improve at low growth temperature (Figure 50).

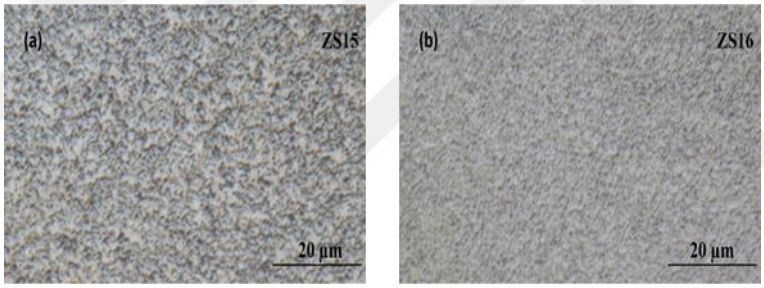

Figure 50. Nomarski microscopy images of (a) ZS15 and (b) ZS16

Figure 51 shows surface morphology of growth ZnSe epitaxial film with and without As sending for same growth temperature. While As was send to surface after deoxidation for ZS11 and ZS12 growth, it was not send during ZS4 and ZS6 growth. ZS4 and ZS12 were grown approximately same flux ratio. It can be seen Figure *51* (a) and (b) that the surface morphology of ZS4 is better than ZS12.When flux ratio was 4 for ZS6 and ZS11, ZS6 has better surface quality than ZS11 in Figure 51 (c) and (d). According to Figure *51*, it can be said that As flux does not effect surface quality well.

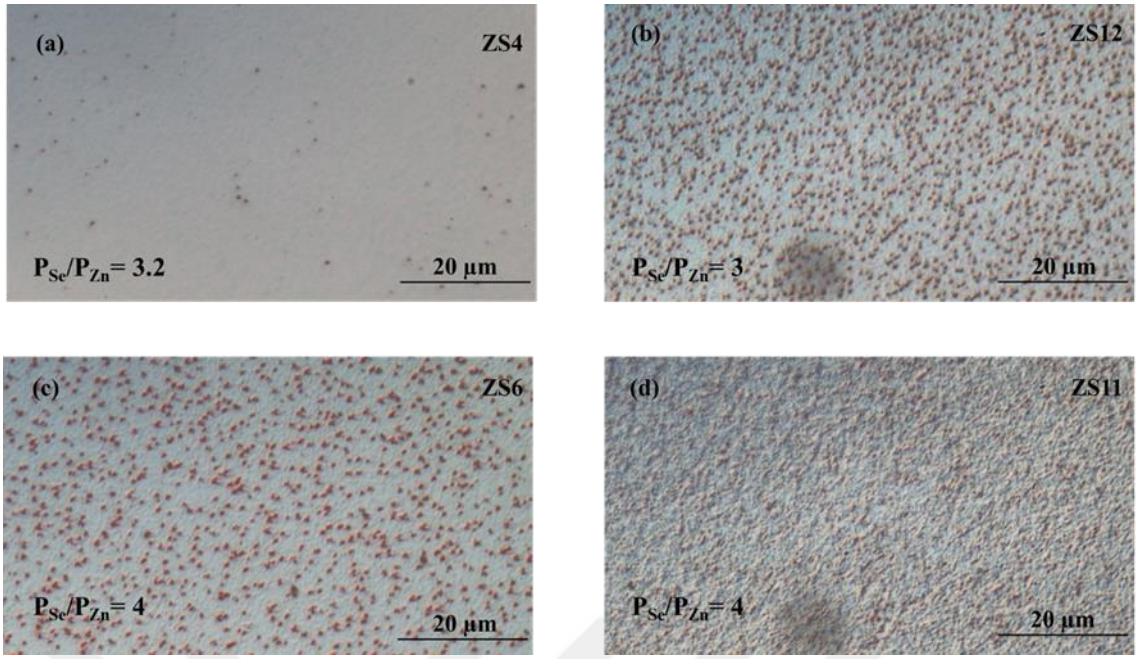

Figure 51. The surface morphologies of ZnSe epitaxial film and (a) ZS4 and (c) ZS6 without As sending, (b) ZS12 and (d) ZS11 with As sending

5.5. Ellipsometry Results

The thickness of ZnSe layer was measured by spectroscopic ellipsometry which is model M-2000X of J.A. Woollam Company. The photon energy range between 1.24 eV and 5.05 eV (or wavelength range between 245 nm and 1000 nm).

In order to obtain film thickness of ZnSe, optical model requires. The optical model consists of dielectric function of each layer. By using dielectric function of materials, which include in SE software library, thickness values were obtained. Dielectric function were used e_1 and e_2, instead of ε_1 and ε_2. Experimental and model data of the pseudo-dielectric function of ZnSe grown on GaAs(211)B (sample ZS1) is given in Figure 52. Red line solid means experimental real part of pseudo-dielectric function (e_1) and green line solid means experimental imaginary part of pseudo-dielectric function (e_2). The model data of pseudo-dielectric is dashed black line. According to fit parameter of this model, the thickness of ZnSe was obtained 1195.9 nm.

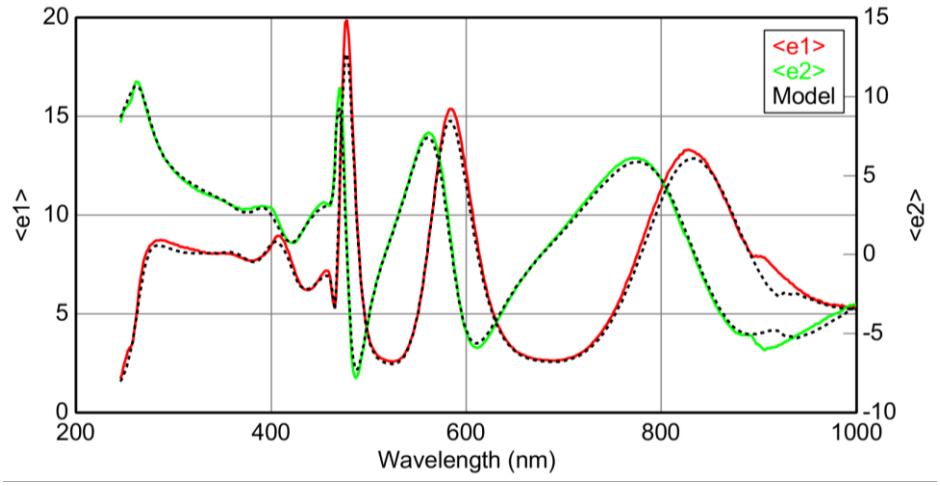

Figure 52. Experimental and Woollam model fit data of pseudo-dielectric function of ZS1 grown on GaAs.

The thickness and growth rate of ZnSe epilayer are given in

Table 11. Growth temperature and time and flux ratio affected these values. When the flux ratio was increased, the quantity of Se and Zn atoms were increased on the substrate. So the film thickness as well.

Table 11.The thickness and some growth parameter of ZnSe layer grown on GaAs(211)B

Sample Name	**VI/II ratio**	**Growth Temperature (^{0}C)**	**Growth Time (min.)**	**Thickness (µm)**	**Growth Rate (µm/hour)**
ZS1	1,7	276	120	0,360	0,18
ZS2	1,8	278	120	0,410	0,205
ZS4	3	300	120	0,440	0,22
ZS10	2	300	120	1,945	0,972
ZS11	4	300	120	2,482	1,241
ZS12	3	300	120	0,649	0,324
ZS13	3	300	120	0,604	0,302
ZS15	3	300	180	1,195	0,398
ZS16	3	272	180	1,292	0,430
ZS17	4	275	180	1,527	0,509

Pseudo dielectric functions were selected as electronvolt dependent to oscillation to obtain oscillations which are used to determine film thickness. When the oscillations becomes more frequently, ZnSe film thickness is increased. It can be seen in Figure 53, Figure 54 and Figure 55.

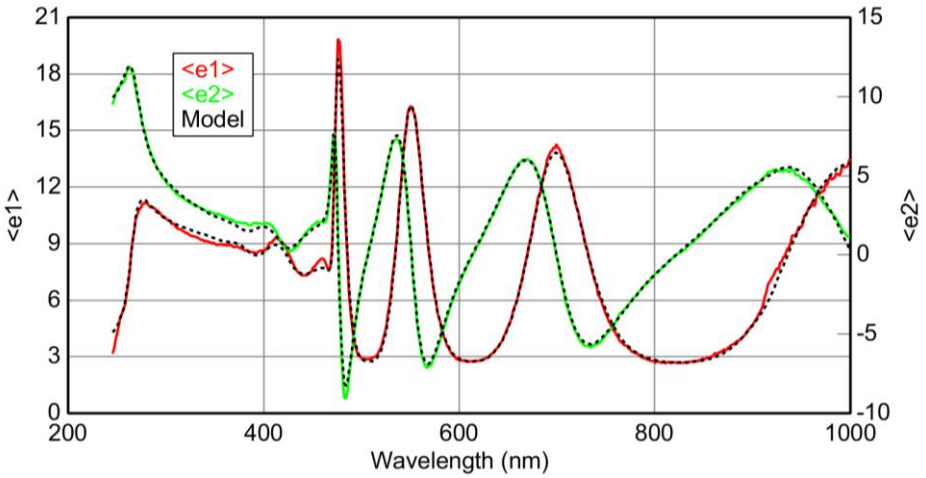

Figure 53. <e1> and <e2> versus energy for ZS4 (440 nm).

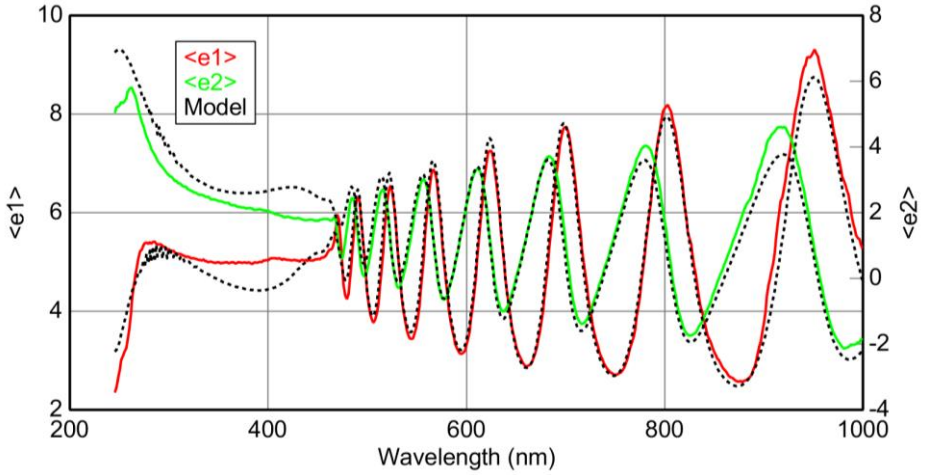

Figure 54. <e1> and <e2> versus energy for ZS15 (1195nm).

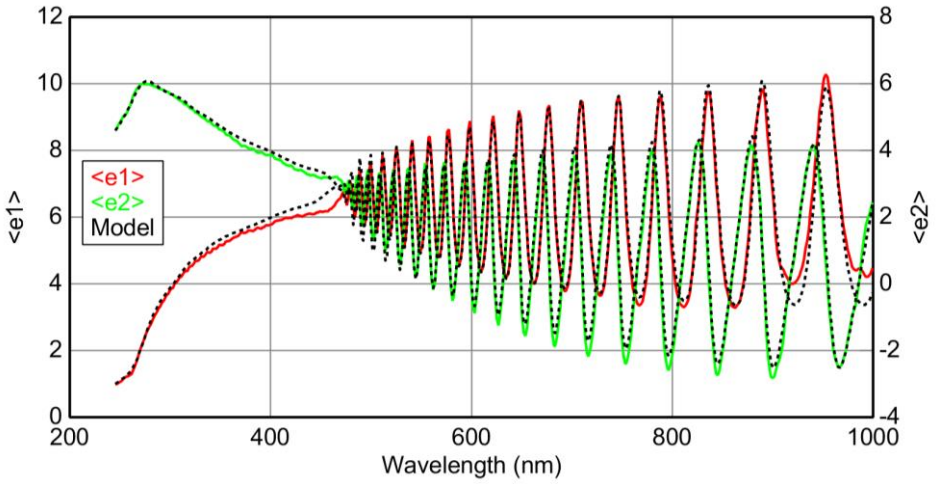

Figure 55. <e1> and <e2> versus energy for ZS11 (2482nm).

5.5. Raman Results

LO phonon frequency of ZnSe epilayer grown on GaAs(211)B was measured from 300K to 80K by using raman spectroscopy. Raman spectra were obtained by Ar^{+}-ion 488 nm excitation laser of maximum is about 12 mW with a 700 nm focal length grating at 1800 gr/mm grating. The light was send on sample with 100x objective and Raman scattered light was detected by Si detector with resolution of 0.3 cm^{-1}.

Strain, happen lattice mismatch, are dominant at high temperature whereas thermal strain, happen difference thermal expansion coefficient between substrate and thin film, are dominant at low temperature. Therefore the Raman measurements were taken to observe strain at different temperature which were 300K and 80K.

Figure 56 shows typical Raman spectrum of ZnSe. The thickness of ZS2 is 0.410 µm and measurement was taken at 300K. This spectrum has LO and TO phonon band of ZnSe and GaAs. 268.715 and 291.856 are TO and LO phonon modes of GaAs respectively. 206.249 and 252.434 cm^{-1} are TO and LO phonon modes of ZnSe respectively. According to literature, calculation of ZnSe TO and LO modes are 250 and 205 cm^{-1}. LO phonon mode of ZnSe shift was 2.434 cm^{-1} for ZS2.

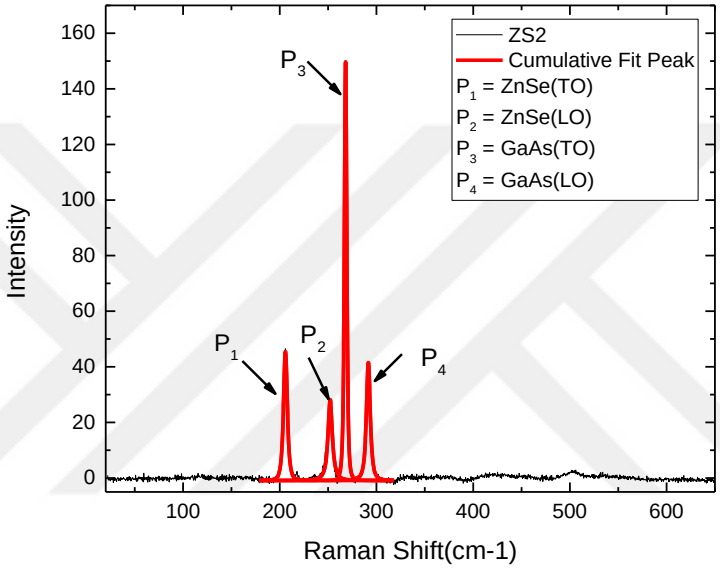

Figure 56. Raman spectrum of ZS2 thin film on GaAs substrate with thickness of 0.410µm at 300K

Figure 57, the effect of flux ratio on Raman shift frequency was investigated. The measurements was taken at 300K and 80K. The flux ratio was changed between 3 and 5, sample were grown without As which means As was not send to surface after deoxidation. Raman shift frequency was decreased when flux ratio was increased.

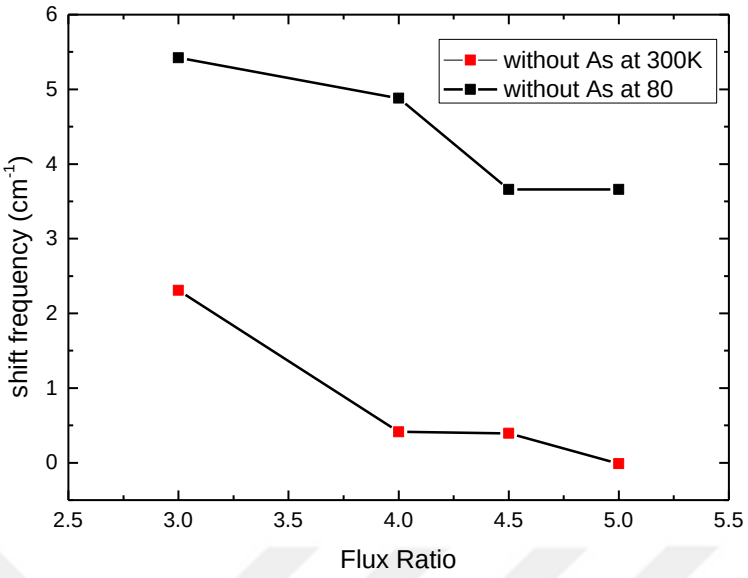

Figure 57. Raman shift frequency of LO phonon for ZnSe thin film with different flux ratio at 300K and 80K

CHAPTER 6

CONCLUSION

The samples were grown by using Molecular Beam Epitaxy (MBE). Flux ratio, growth temperature and deoxidation process were studied during the experiment. Before the growth, native oxide of GaAs(211)B substrate was deoxized two different elements, were In and As. After that growths were done various flux ratio. The film thickness was measured with Spectroscopic Ellipsometry(SE). When flux ratio and growth time were increased, film thickness increased.

To obtain crystalline quality of as-grown ZnSe epilayer, X-ray diffraction (XRD) measurements were performed. X-ray rocking curve of FWHM was depend on the flux ratio. The FWHM of ZnSe epilayer film increased when the flux ratio was increased. It means that tilted and strain start to happen in the film. The effect of As flux on crystal quality of film was studied. While the deoxidation process was being done, some As atoms removed on the surface. These As defiency may be affect crystal quality of ZnSe epilayer film. Hence As was send in a few minute after deoxidation process finished. ZS12 and ZS13 were grown with same flux ratio and growth temperature. Difference between them As was not send while ZS13 was grown. When the FWHM of these two samples were looked, the FWHM of ZS13 was smaller than ZS12. Hence As did not improved crystal quality of ZnSe epilayer. And also the affect of growth temperature was examined on FWHM of ZnSe epilayer film. ZS15 and ZS16 were grown with same flux ratio but growth temperatures were different. At high growth temperature FWHM was smaller than at low temperature.

The surface morphology of as-grown ZnSe epilayer were estimated Nomarski microscopy. The effect of growth temperature on epitaxial growth of ZnSe films were seen. Defects was increased at low temperature and it started to decrease when the growth temperature was increased. Topographic images of as-grown ZnSe epilayer were taken with AFM and the average RMS roughness was calculated by taking three different scanned regions. The oxide of substrates were removed In. It was seen that roughness values were increased approximately until 4 flux ratio after it started to reduce. Also after deoxidation process finished, As flux was send to substrate to fulfil

deficiency of As atoms in substrate. The surface morphology did not improve with As flux when compared to without As.

Raman spectroscopy was used to observe vibrational phonon mode, thermal and elastic strain of as-grown ZnSe epilayer. Thermal strain is dominant at low temperature and elastic strain is dominant at high temperature. Hence the measurements were taken 300K and 80K. Raman shift frequency of ZnSe LO phonon mode was examined when flux ratio was changed. The shift frequency was decreased with increasing flux ratio when the measurement was taken at 80K. It means that strain started to decrease in the film.

Finally, the best crystal and surface crystal quality were obtained for ZS4 which was grown with 3 flux at 300^0C. Its film thickness is 0.444 μm. It can be said that high growth temperature and 3 flux ratio is suitable to obtain good quality of ZnSe epilayer.

.

REFERENCES

1. Arias, J., et al., *Dislocation density reduction by thermal annealing of HgCdTe epilayers grown by molecular beam epitaxy on GaAs substrates.* Journal Of Vacuum Science & Technology B, 1991. 9(3): p. 1646-1650.

2. Lennon, C., et al., *Real-Time In Situ Monitoring of GaAs (211) Oxide Desorption and CdTe Growth by Spectroscopic Ellipsometry.* Journal of electronic materials, 2012. 41(10): p. 2965-2970.

3. Kumazaki, K., K. Imai, and A. Odajima, *Estimation of Strains in MBE-Grown ZnSe Films by Raman Scattering.* physica status solidi (a), 1990. 119(1): p. 177-182.

4. Rogalski, A., *HgCdTe infrared detector material: history, status and outlook.* Reports on Progress in Physics, 2005. 68(10): p. 2267.

5. He, L., et al., *MBE HgCdTe on alternative substrates for FPA applications.* Journal of Electronic Materials, 2008. 37(9): p. 1189-1199.

6. He, L., et al., *MBE HgCdTe on Si and GaAs substrates.* Journal of Crystal Growth, 2007. 301: p. 268-272.

7. Jacobs, R., et al., *Development of MBE II–VI Epilayers on GaAs (211) B.* Journal of electronic materials, 2012: p. 1-7.

8. Sporken, R., et al., *Molecular beam epitaxial growth of CdTe and HgCdTe on Si (100).* Applied Physics Letters, 1989. 55(18): p. 1879-1881.

9. Zanatta, J., et al., *Molecular beam epitaxy growth of HgCdTe on Ge for third-generation infrared detectors.* Journal of electronic materials, 2006. 35(6): p. 1231-1236.

10. Johnson, S.M., et al., *Effect of dislocations on the electrical and optical properties of long-wavelength infrared HgCdTe photovoltaic detectors.* Journal of Vacuum Science & Technology B: Microelectronics and Nanometer Structures Processing, Measurement, and Phenomena, 1992. 10(4): p. 1499-1506.

11. Carmody, M., et al., *LWIR HgCdTe on Si detector performance and analysis.* Journal of electronic materials, 2006. 35(6): p. 1417-1422.

12. Beamer, W.H. and C.R. Maxwell, *Physical Properties of Polonium. II. X-Ray Studies and Crystal Structure.* The Journal of Chemical Physics, 1949. 17(12): p. 1293-1298.

13. Bilgilisoy, E., *Characterization of lattice mismatch induced dislocations on epitaxial CdTe films*. 2015, İzmir Institute of Technology.

14. Mao, H.K., W.A. Bassett, and T. Takahashi, *Effect of pressure on crystal structure and lattice parameters of iron up to 300 kbar.* Journal of Applied Physics, 1967. 38(1): p. 272-276.

15. Brillouin, L., *Wave propagation in periodic structures: electric filters and crystal lattices*. 2003: Courier Corporation.

16. Vogl, á., H.P. Hjalmarson, and J.D. Dow, *A semi-empirical tight-binding theory of the electronic structure of semiconductors.* Journal of Physics and Chemistry of Solids, 1983. 44(5): p. 365-378.

17. Lagakos, N., J. Cole, and J.A. Bucaro, *Microbend fiber-optic sensor.* Applied Optics, 1987. 26(11): p. 2171-2180.

18. Bauer, E., *Epitaxy of metals on metals.* Applications of surface science, 1982. 11: p. 479-494.

19. Dean, P., et al., *Ionization energy of the shallow nitrogen acceptor in zinc selenide.* Physical Review B, 1983. 27(4): p. 2419.

20. Feng, M., et al., *Tunnel junction transistor laser.* Applied Physics Letters, 2009. 94(4): p. 041118.

21. VERMA, P., et al., *Optical Identification of Cu Doped ZnSe Nanoparticles.* Journal of Pure Applied and Industrial Physics Vol, 2011. 1(4): p. 212-277.

22. Coronado, C.A., *Growth and characterization of ZnSe by metalorganic and gas source molecular beam epitaxy*. 1994, Massachusetts Institute of Technology.

23. Haase, M., et al., *Blue-green laser diodes.* Applied Physics Letters, 1991. 59(11): p. 1272-1274.

24. Park, R. and H. Mar, *Growth and photoluminescence characterization of ZnSe layers grown on (100) Ge by molecular beam epitaxy.* Journal of Materials Research, 1986. 1(04): p. 543-546.

25. Yamaguchi, E., et al., *Growth of ZnSe on Ge (100) substrates by molecular-beam epitaxy.* Journal of applied physics, 1987. 62(3): p. 885-889.

26. Reichow, J., et al., *Molecular beam epitaxial growth and characterization of ZnSe on GaAs.* Journal of crystal growth, 1993. 131(3-4): p. 277-282.

27. Koh, K., et al., *Growth of ZnSe on GaAs (110) surfaces by molecular beam epitaxy.* Journal of crystal growth, 1998. 186(4): p. 528-534.

28. Park, R. and H. Mar, *Molecular beam epitaxial growth of high quality ZnSe on (100) Si.* Applied physics letters, 1986. 48(8): p. 529-531.

29. Bringans, R., et al., *Effect of interface chemistry on the growth of ZnSe on the Si (100) surface.* Physical Review B, 1992. 45(23): p. 13400.

30. Li, L., et al., *Molecular beam epitaxial growth of single domain ZnSe on Ge.* Journal of applied physics, 1994. 75(4): p. 2026-2028.

31. http://www.semiconductors.co.uk/propiiiv5653.htm, Accessed June 06, 2016.

32. http://www.semiconductors.co.uk/propiviv5431.htm, Accessed June 06, 2016.

33. Romano, L., et al., *Misfit dislocations in ZnSe grown on vicinal Si (001) substrates.* Applied physics letters, 1994. 65(7): p. 869-871.

34. Bringans, R., et al., *Effect of interface chemistry on the growth of ZnSe on the Si (100) surface.* Physical Review B, 1992. 45(23): p. 13400.

35. Opel, M., *Spintronic oxides grown by laser-MBE.* Journal of Physics D: Applied Physics, 2011. 45(3): p. 033001.

36. Chen, Y., et al., *MBE-grown ZnTe/Si, a low-cost composite substrate.* Journal of electronic materials, 2012. 41(10): p. 2917-2924.

37. Aoki, T., et al., *ZnSe epitaxial growth on Si (100) and Ge (100) by H-radical assisted MOCVD.* Applied surface science, 1997. 113: p. 23-27.

38. Wang, W., *Molecular beam epitaxial growth and material properties of GaAs and AlGaAs on Si (100).* Applied Physics Letters, 1984. 44(12): p. 1149-1151.

39. Kroemer, H., *Polar-on-nonpolar epitaxy.* Journal of Crystal Growth, 1987. 81(1): p. 193-204.

40. Fischer, R., et al., *Material properties of high-quality GaAs epitaxial layers grown on Si substrates.* Journal of applied physics, 1986. 60(5): p. 1640-1647.

41. Park, R., J. Kleiman, and H. Mar. *Molecular Beam Epitaxial Growth Of ZnSe On (100) GaAs And (100) Ge: A Comparative Study Of Material Quality*. in *Semiconductor Conferences*. 1987. International Society for Optics and Photonics.

42. Itsuno, A.M., *Bandgap-engineered HgCdTe infrared detector structures for reduced cooling requirements*. 2012, The University of Michigan.

43. Kim, J.J., et al., *TEM characterization of HgCdTe/CdTe grown on GaAs (211) B substrates.* Journal of electronic materials, 2013. 42(11): p. 3142.

44. Kissinger, S., N. Velmuruganb, and K. Perumalc, *Substrate temperature dependent structural and optical properties of ZnSe thin films by electron beam evaporation technique.* Journal of Korean Physical Society, 2009. 55: p. 1577.

45. Okuyama, H., et al., *Epitaxial growth of ZnMgSSe on GaAs substrate by molecular beam epitaxy.* Japanese journal of applied physics, 1991. 30(9B): p. L1620.

46. Jeon, H., et al., *Blue-green injection laser diodes in (Zn, Cd) Se/ZnSe quantum wells.* Applied physics letters, 1991. 59(27): p. 3619-3621.

47. Kim, M.J., et al., *Physical Properties of ZnSe Thin Films Depending on the Process Parameters.* Molecular Crystals and Liquid Crystals, 2013. 586(1): p. 129-137.

48. Yan, L., J.A. Woollam, and E. Franke, *Oxygen plasma effects on optical properties of ZnSe films.* Journal of Vacuum Science & Technology A, 2002. 20(3): p. 693-701.

49. Kim, T. and H. Lee, *Effect of a ZnSe buffer layer on the surface, structural, and optical properties of the ZnTe/ZnSe/GaAs heterostructures.* Materials research bulletin, 2002. 37(10): p. 1763-1771.

50. Hishida, Y., T. Toda, and T. Yamaguchi, *Characteristics of Li-and Cl-doped ZnTe grown by molecular beam epitaxy.* Journal of crystal growth, 1992. 117(1): p. 396-399.

51. Ohtsuka, T., et al., *Low resistance ohmic contact for p-type ZnTe using Au electrode.* Applied physics letters, 1995. 67(9): p. 1277-1279.

52. Mackey, K., et al., *Semiconductor-semiconductor heterojunctions; The application of surface science techniques to study InSb/ CdTe surfaces and their interfaces.* Surface Science, 1986. 178(1): p. 124-130.

53. Kim, T., et al., *R. f. C. FARROW, T. TEMOFONTE, F A. SHIRLAND and A. NOREIKA.* J. Vacuum Sci. Technol. B, 1987. 5: p. 980.

54. Kim, T., et al., *Interfacial layer formation of the CdTe/InSb heterointerfaces grown by temperature gradient vapor transport deposition.* Applied physics letters, 1994. 65(20): p. 2597-2599.

55. Sochinskii, N., et al., *Substrate effect on CdTe layers grown by metalorganic vapor phase epitaxy.* Applied physics letters, 1997. 70(10): p. 1314-1316.

56. Qiu, Y., et al., *Growth modes of ZnSe on GaAs.* Journal of applied physics, 1996. 79(2): p. 1164-1166.

57. Guha, S., H. Munekata, and L. Chang, *Structural quality and the growth mode in epitaxial ZnSe/GaAs (100).* Journal of applied physics, 1993. 73(5): p. 2294-2300.

58. Reichow, J., et al., *Molecular beam epitaxial growth and characterization of ZnSe on GaAs.* Journal of crystal growth, 1993. 131(3): p. 277-282.

59. Gaines, J., J. Petruzzello, and B. Greenberg, *Structural properties of ZnSe films grown by migration enhanced epitaxy.* Journal of applied physics, 1993. 73(6): p. 2835-2840.

60. Nakashima, S.-i., et al., *Raman scattering measurements of strains in ZnSe epitaxial films on GaAs.* Japanese journal of applied physics, 1988. 27(7R): p. 1327.

61. Callister, W.D. and D.G. Rethwisch, *Materials science and engineering*. Vol. 5. 2011: John Wiley & Sons NY.

62. http://archive.cnx.org/contents/0b2614e4-aa98-49c1-bf50-1db3ee3c5ecd@2/molecular-beam-epitaxy, Accessed October 17, 2016.

63. http://goo.gl/Uv5y8H, Accessed November 15, 2016.

64. https://www.physik.uni-kl.de/hillebrands/research/methods/molecular-beam-epitaxy/, Accessed October 18, 2016.

65. Culver, W., J. Vanderslice, and V. Townsend, *Controlled Generation of Intense Light Pulses in Reverse-Pumped Raman Lasers.* Applied Physics Letters, 1968. 12(5): p. 189-190.

66. http://www.ifm.liu.se/courses/tfyy36/pdf/TFYY36_L6.pdf, Accessed January 14, 2017.

67. http://csmantech.org/OldSite/Digests/2013/papers/032.pdf, Accessed January 20 2017.

68. Mitsuhashi, H., et al., *Coherent growth of ZnSe on GaAs by MOCVD.* Japanese journal of applied physics, 1985. 24(8A): p. L578.

69. https://www.google.com.tr/webhp?sourceid=chrome-instant&ion=1&espv=2&ie=UTF-8#q=ald+process+and+equipment+ppt, Accessed January 05, 2017.

70. Yao, T. and T. Takeda, *Growth process in atomic layer epitaxy of Zn chalcogenide single crystalline films on (100) GaAs.* Applied physics letters, 1986. 48(2): p. 160-162.

71. Suntola, T. and J. Antson, *Method for producing compound thin films*. 1977, Google Patents.

72. http://groups.ist.utl.pt/rschwarz/rschwarzgroup_files/PLD_files/PLD.htm, Accessed January 10, 2017.

73. Ryu, Y., et al., *Optical and structural properties of ZnO films deposited on GaAs by pulsed laser deposition.* Journal of Applied Physics, 2000. 88(1): p. 201-204.

74. http://www.veeco.com/products/gen20-mbe-system, Accessed February 09, 2017.

75. Biasiol, G. and L. Sorba, *Molecular beam epitaxy: principles and applications.* Crystal growth of materials for energy production and energy-saving applications, 2001: p. 66-83.

76. http://www.spts.com/tech-insights/mems/mems-microphones, Accessed February 09, 2017.

77. Drude, P., *Bestimmung der optischen Constanten der Metalle.* Annalen der Physik, 1890. 275(4): p. 481-554.

78. Rothen, A., *The ellipsometer, an apparatus to measure thicknesses of thin surface films.* Review of Scientific Instruments, 1945. 16(2): p. 26-30.

79. Cahan, B. and R. Spanier, *A high speed precision automatic ellipsometer.* Surface Science, 1969. 16: p. 166-176.

80. Collins, R., *Automatic rotating element ellipsometers: Calibration, operation, and real-time applications.* Review of Scientific Instruments, 1990. 61(8): p. 2029-2062.

81. http://www.jawoollam.com/pdf/CompleteEASE_Brochure.pdf., accessed January 06, 2017.

82. http://glossary.periodni.com/glossary.php?en=Lennard-Jones+potential, Accessed October 14, 2016.

83. http://www.eng.utah.edu/~lzang/images/Lecture_10_AFM.pdf, Accessed October 14, 2016.

84. https://application.wiley-vch.de/books/sample/3527334637_c01.pdf, Accessed December 12, 2016.

85. http://www.physik.fu-berlin.de/studium/praktika-forward/fpa_dipl-ws2009/docs/Ma7_Raman.pdf, Accessed November 06, 2016.

86. Farrer, I., et al., *Substrate temperature measurement using a commercial band-edge detection system.* Journal of Crystal Growth, 2007. 301: p. 88-92.

87. Ko, H.-C., et al., *Optimization of ZnSe growth on the cleavage-induced GaAs (1 1 0) surface by molecular-beam epitaxy.* Journal of crystal growth, 1997. 178(3): p. 246-251.